IGNITION RATE MEASUREMENT OF LASER-IGNITED COALS

FINAL TECHNICAL REPORT

08/01/97 TO 07/31/97

AUTHORS: JOHN C. CHEN
VINAYAK KABADI

REPORT ISSUE DATE: 10/31/97

DE-FG22-94MT94012 --12

NORTH CAROLINA A&T STATE UNIVERSITY
DEPARTMENT OF MECHANICAL ENGINEERING
1601 E. MARKET STREET
GREENSBORO, NC 27411

Disclaimer

This report was prepared as an account of work sponsored by an agency of the United States Government. Neither the United States Government nor any agency thereof, nor any of their employees, makes any warranty, express or implied, or assumes any legal liability or responsibility for the accuracy, completeness, or usefulness of any information, apparatus, product, or process disclosed, or represents that its use would not infringe privately owned rights. Reference herein to any specific commercial product, process, or service by trade name, trademark, manufacturer, or otherwise does not necessarily constitute or imply its endorsement, recommendation, or favoring by the United States Government or any agency thereof. The views and opinions of authors expressed herein do not necessarily state or reflect those of the United States Government or any agency thereof.

Abstract

We have established a novel experiment to study the ignition of pulverized coals under conditions relevant to utility boilers. Specifically, our aims were to determine the ignition mechanism, which is either homogeneous or heterogeneous, of pulverized coal particles under various conditions of particle size, coal type, and freestream oxygen concentration. Furthermore, we will measure the ignition rate constants of various coals by direct measurement of the particle temperature at ignition, and incorporating this measurement into a mathematical model for the ignition process. All of the above objectives were met by the project.

The ignition mechanism of pulverized coals in this experiment, under all conditions examined, was determined by high-speed photography to be *heterogeneous*. That is, ignition of the particles always occurred on the solid surface, prior to the evolution of volatile matter from the particles into the gas phase. This finding was most likely due to the high heating rates achieved ($>10^5$) by the laser heating, which causes the particle temperature to rise above that necessary for ignition before appreciable devolatilization occurred.

Particle temperature at ignition was measured for one size group of one coal (Pittsburgh #8, high-volatile bituminous) under two oxygen concentrations. These temperatures were analyzed using a model of heterogeneous coal ignition developed by our group, and ignition rate constants were determined.

Table of Contents

Executive Summary

We established a novel experiment to study the ignition of pulverized coals under conditions relevant to utility boilers. Specifically, we determined the ignition mechanism of pulverized-coal particles under various conditions of particle size, coal type, and freestream oxygen concentration. We also measured the ignition rate constant of a Pittsburgh #8 high-volatile bituminous coal by direct measurement of the particle temperature at ignition, and incorporating this measurement into a mathematical model for the ignition process. The model, called Distributed Activation Energy Model of Ignition, was developed previously by our group to interpret conventional drop-tube ignition experiments, and was modified to accommodate the present study.

We constructed a laser-based apparatus that offers several advantages over drop-tube furnace experiments, which are currently in favor. Sieve-sized particles were dropped batch-wise into a laminar, upward-flow wind tunnel that is constructed with a quartz test section. The gas stream was not preheated. A single pulse from a Nd:YAG laser was focused through the tunnel and ignites several particles. The transparent test section and cool walls allowed for application of two-color pyrometry to measure the particles' temperature history during ignition and combustion. For each fuel type, measurements of the ignition temperature under various experimental conditions (particle size and free-stream oxygen concentration), combined with a detailed analysis of the ignition process, permitted the determination of kinetic rate constants of ignition.

This technique offers many advantages over conventional experiments. One is the ability to directly measure ignition temperature rather than inferring it from measurements of the minimum *gas temperature* needed to induce ignition. Another advantage is the high heating rates achievable – on the order of 10^6 K/s. This is a significant improvement over experiments that rely on convective heating from a hot gas, which typically achieves heating rates of 10^4 K/s. The higher

heating rate more closely simulates conditions in conventional coal combustors used for power generation.

It should be noted that single-particle behavior governs the conditions of this experiment; i.e., the particle suspension is dilute enough that particle-to-particle effects (other than radiative heat transfer) are not important. In actual combustors, particle loading, especially near the injector, is high enough that such "cooperative effects" dominate.

The ignition mechanism of pulverized coals in this experiment, under all conditions examined, was determined by high-speed photography to be *heterogeneous*. That is, ignition of the particles always occurred on the solid surface, prior to the evolution of volatile matter from the particles into the gas phase. This finding was most likely due to the high heating rates achieved ($>10^5$) by the laser heating, which causes the particle temperature to rise above that necessary for ignition before appreciable devolatilization occurred.

Ignition-frequency distributions for four coals (one subbituminous, two high-volatile bituminous, and one medium-volatile bituminous) are presented. The experimental conditions examined include variation of particle size, oxygen concentration, and laser-pulse energy. The distributions show clearly that ignition behavior is dominated by particle-to-particle variation in reactivity and is perhaps influenced by size as well.

Particle temperature at ignition was measured for one size group (125-150 μm) of one coal (Pittsburgh #8, high-volatile bituminous) under two oxygen concentrations. At 100% oxygen, the ignition temperature of this coal was found to be 1310 K, while at 50% oxygen the ignition temperature was 1460 K. The higher temperature was expected since, for a lower oxygen level, a higher temperature is needed to cause particle ignition. Also, it was found that a distribution of ignition temperature exists at each experimental condition. This is believed to be a result of the particle-to-particle variations in reactivity and size among the coal sample.

The measured ignition temperatures were analyzed using the Distributed Activation Energy Model of Ignition, and the ignition rate constant was determined to have an average value of 73 kJ/mol with a standard deviation of 3.7 kJ/mol. It is imperative to collect an extensive set of ignition data in order to establish meaningful statistics for the extraction of ignition rate constants. We plan to continue this study and to collect the data just described. Additionally, we make an extensive set of recommendations for future work.

Introduction

Over the last several decades many experiments have been conceived to study the ignition of pulverized coal and other solid fuels. We constructed a laser-based apparatus that offers several advantages over those currently in favor. Sieve-sized particles are dropped batch-wise into a laminar, upward-flow wind tunnel that is constructed with a quartz test section. The gas stream is not preheated. A single pulse from a Nd:YAG laser is focused through the tunnel and ignites several particles. The transparent test section and cool walls allow for application of two-color pyrometry to measure the particles' temperature history during ignition and combustion. Coals ranging in rank from lignites to low-volatile bituminous, and chars derived from these coals, will be studied in this project. For each fuel type, measurements of the ignition temperature under various experimental conditions (particle size and free-stream oxygen concentration), combined with a detailed analysis of the ignition process, will permit the determination of kinetic rate constants of ignition.

This technique offers many advantages over conventional drop-tube furnace experiments. One is the ability to directly measure ignition temperature rather than inferring it from measurements of the minimum *gas temperature* needed to induce ignition. Another advantage is the high heating rates achievable — on the order of 10^6 K/s. This is a significant improvement over experiments which rely on convective heating from a hot gas, which typically achieves heating rates of 10^4 K/s. The higher heating rate more closely simulates conditions in conventional coal combustors used for power generation.

It should be noted that single-particle behavior governs the conditions of this experiment; i.e., the particle suspension is dilute enough that particle-to-particle effects (other than radiative heat transfer) are not important. In actual combustors, particle loading, especially near the injector, is high enough that such "cooperative effects" dominate. Our approach is to gain a clear

understanding of single-particle behavior with this experiment, before facing the more difficult problem encountered with cloud suspensions.

Our main motivations for this project are to determine the ignition mechanism of various coals and to measure the ignition rate constant of a range of coals under single-particle conditions. Our long-range, ultimate objectives are to (1) describe the ignition behavior of coals in a suspension, (2) predict the ignition behavior of blend(s) of coals in a suspension, and (3) apply these predictive tools in the design of burners and boiler units.

Objectives

Our specific, overall objectives for this project are:

1. Construction of the laser-ignition experiment, including:
   1.1. gas delivery and regulation system;
   1.2. wind tunnel;
   1.3. exhaust system;
   1.4. laser system and beam-guiding optics;
   1.5. optical detection system; and
   1.6. data acquisition and processing;
2. Shakedown testing of the various components;
3. Ignition of coals of various rank, from lignites to low-volatile bituminous;
4. Measurement of the ignition temperatures of these fuels under various experimental conditions (particle size and free-stream oxygen concentration);
5. Extraction of ignition rate constants from temperature measurements by application of an appropriate heterogeneous-ignition analysis.

Results and Discussion

I. Experiment Development

A. Experiment Overview

Figure 1 presents a schematic of the laser ignition experiment; the inset shows the details around the test section. Sieve-sized particles were dropped through a tube into a laminar, upward-flow wind tunnel with a quartz test section (5 cm square cross-section). The gas was not preheated. The gas flow rate was set so that the particles emerged from the feeder tube, fell approximately 5 cm, then turned and traveled upward out of the tunnel. This ensured that the particles were moving slowly downward at the ignition point, chosen to be 3 cm below the feeder-tube exit. A single pulse from a Nd:YAG laser was focused through the test section, then defocused after exiting the test section, and two addition prisms folded the beam back through the ignition point. Heating the particles from two sides in this manner achieved more spatial uniformity and allowed for higher energy input than a single laser pass. For nearly every case, two to five particles were contained in the volume formed by the two intersecting beams, as determined by observation with high-speed video.

The laser operated at 10 Hz and emitted a nearly collimated beam (6 mm diameter) in the near-infrared (1.06 μm wavelength). The laser pulse duration was ~100 μs and the pulse energy was fixed at 830 mJ per pulse, with pulse-to-pulse energy fluctuations of less than 3%. The laser pulse energy delivered to the test section was varied by a polarizer placed outside of the laser head; variation from 150 to 750 mJ was achieved by rotating the polarizer. Increases in the laser pulse energy resulted in heating of the coal particles to higher temperatures. At the ignition point the beam diameter normal to its propagation direction was ~3 mm on each pass of the beam. An air-piston-driven laser gate (see Figure 1) permitted the passage of a single pulse to the test section.

The system allowed for control of the delay time between the firing of feeder and the passage of the laser pulse, which was necessary since coal samples of different sizes and/or densities required different time periods to fall through the feeder tube. Finally, ignition or nonignition was determined by examining the signal generated by a high-speed silicon photodiode connected to a digital oscilloscope.

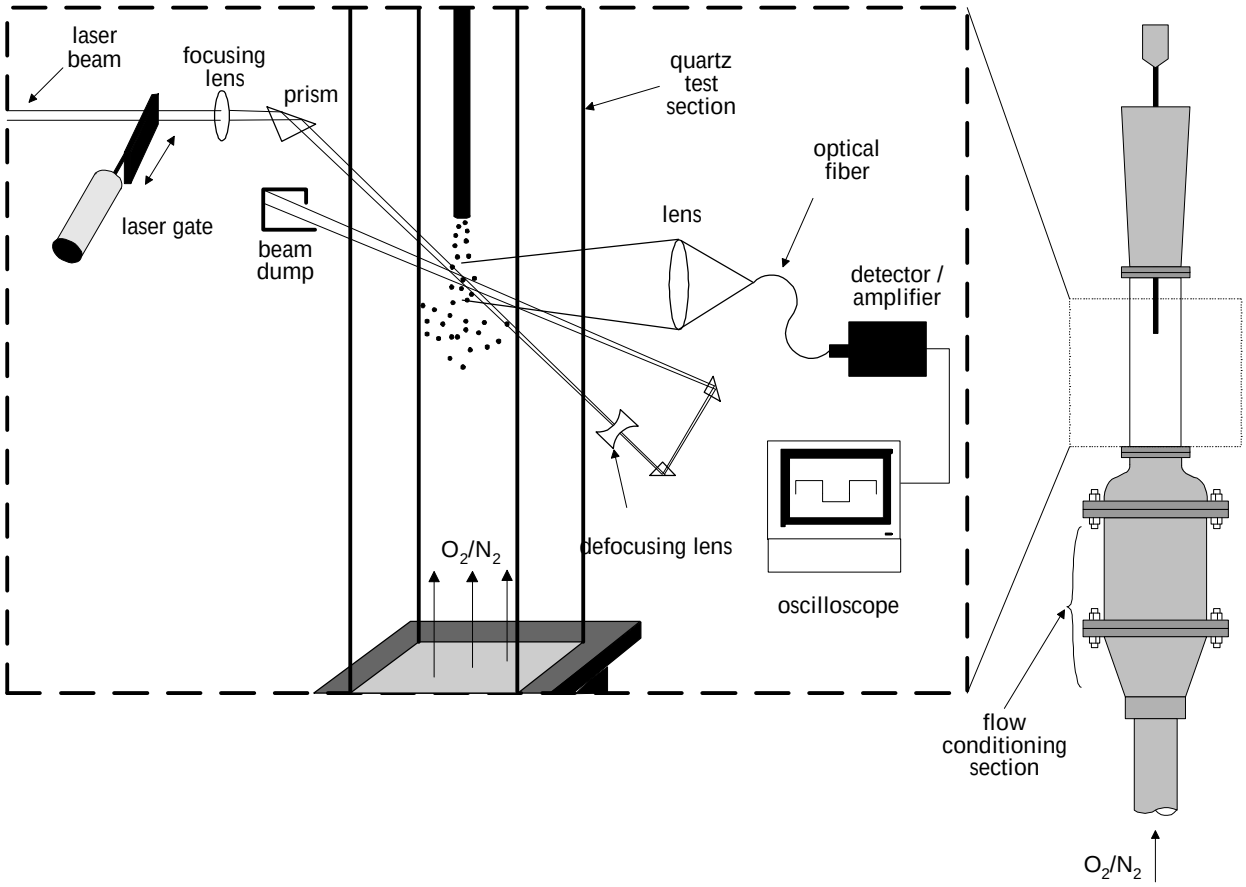

Figure 1: Schematic showing the laser ignition apparatus.

B. Coal preparation and handling

Coals were received from Penn State Coal Sample Bank packed under an argon atmosphere. Approximately 150 gm of coal was transferred into pint jars for vacuum drying at 10 in. Hg and 76°C for 8 hours. Each coal was then dry sieved and stored in small jars kept in desiccator cabinets.

Small quantities of the sample, ~50 gm, were sieved in a single pass using a Ro-Tap sieve shaker. Table 1 shows a list of mesh numbers and their corresponding opening diameters for the sieves used. Since the shaker did not accommodate all eight sieves at the same time, sieving was carried out in two batches. The first four sieves used were 80, 100, 120 and 140 meshes, with 80 mesh at the top and 140 mesh at the bottom. Each time the sieves were shaken for 15 minutes, followed by vacuum suction applied to the underside of each sieve for about a minute, so that fine particles could be removed. The particles on each mesh were then emptied into small bottles for storage. A small brush was used to gently remove any particles which were lodged in the mesh. The remaining sample which passed through the 140 mesh sieve was the starting sample for the second set of sieves (170 mesh at the top and 270 mesh at the bottom). The same procedure was repeated for this set of sieves.

Mesh	Size range of particles retained (μm)
+80	>180
+100	150-180
+120	125-150
+140	106-125
+170	90-106
+200	75-90
+230	63-75
+270	53-63

Table 1: Meshes of sieves used to size coals, and their corresponding nominal mesh openings.

Thus, the coals collected were in mesh sizes: -80/+100, -100/+120, -120/+140, -140/+170, -170/+200, -200/+230, and -230/+270. The +80 and -270 samples were discarded as they were not size classified. This procedure of drying followed by sieving was carried out for each coal and the samples obtained were stored. Six different coals have been prepared for the present study ranging in rank from lignites to low-volatile bituminous (Table 2).

	(Dry wt%)		(Dry, Ash-Free wt%)			
Coal Type	**Volatile Matter**	**Ash**	**C**	**H**	**N**	**O+S (diff)**
DECS 13 Sewell mvb	24.98	4.22	84.47	4.74	1.44	5.13
DECS 19 Pocahontas lvb	18.31	4.60	85.74	4.67	1.09	3.90
DECS 23 Pittsburgh hvAb	39.42	9.44	74.21	5.10	1.35	9.90
DECS 24 Illinois #6 hvCb	40.83	13.39	66.05	4.59	1.14	14.83
DECS 25 Pust lignite A	41.98	11.85	65.76	4.60	0.94	16.85
DECS 26 Wyodak subbituminous	44.86	7.59	69.77	5.65	0.94	16.07

Table 2: Proximate and ultimate analyses of coals used.

The coals were dried in a vacuum oven at 70^{o}C for 24 h prior to use for each day's experiment(s). It is critically important to carefully control the contact between the dried coals and any moisture – in the air and on the hands of handlers – in order to obtain good reproducibility of data from day to day. For this reason, the coals were removed from the oven just prior to running experiments each day, and only one batch was loaded into the coal feeder for each day's use.

C. Gas-handling system

The gas flow system is shown in Figure 2. Oxygen and nitrogen were directed separately through pressure regulators and flowmeters. The two gases were blended in the required ratio and flow rates, and directed to the wind tunnel as a mixture. Figure 3 shows a photograph of the gas flow system.

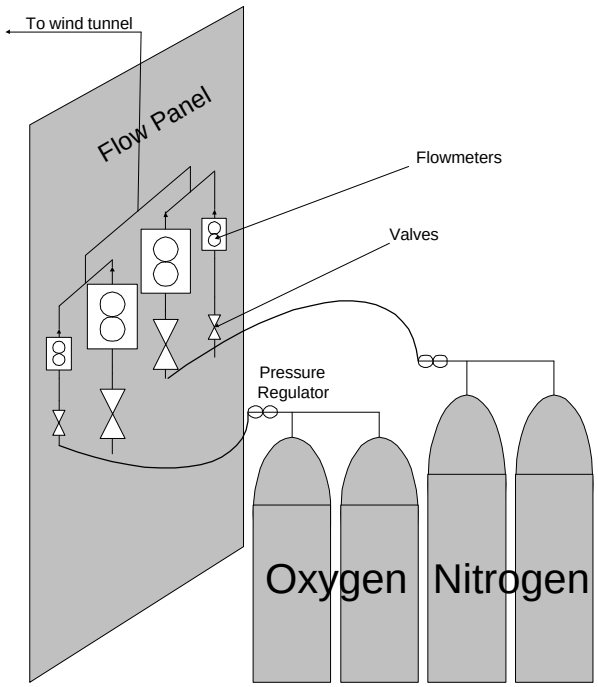

Figure 2: Schematic showing gas-handling system.

Figure 3: Photograph showing the gas-handling system.

D. Wind tunnel

The wind tunnel was constructed as shown in Figure 4. The initial 90^o elbow has a cross section of 57 mm square. A wide-angle diffuser of 122 mm square cross section followed the elbow and expanded the flow into the flow-conditioning section. Two wire meshes and a honeycomb were used in the flow conditioner to reduce turbulence and to straighten the flow. A honeycomb upstream of the test section ensured flow uniformity for some distance downstream. The gas passing through the quartz test section leaves the wind tunnel through the diffuser along with the coal particles. Engineering drawings of the wind tunnel parts are provided in Appendix C.

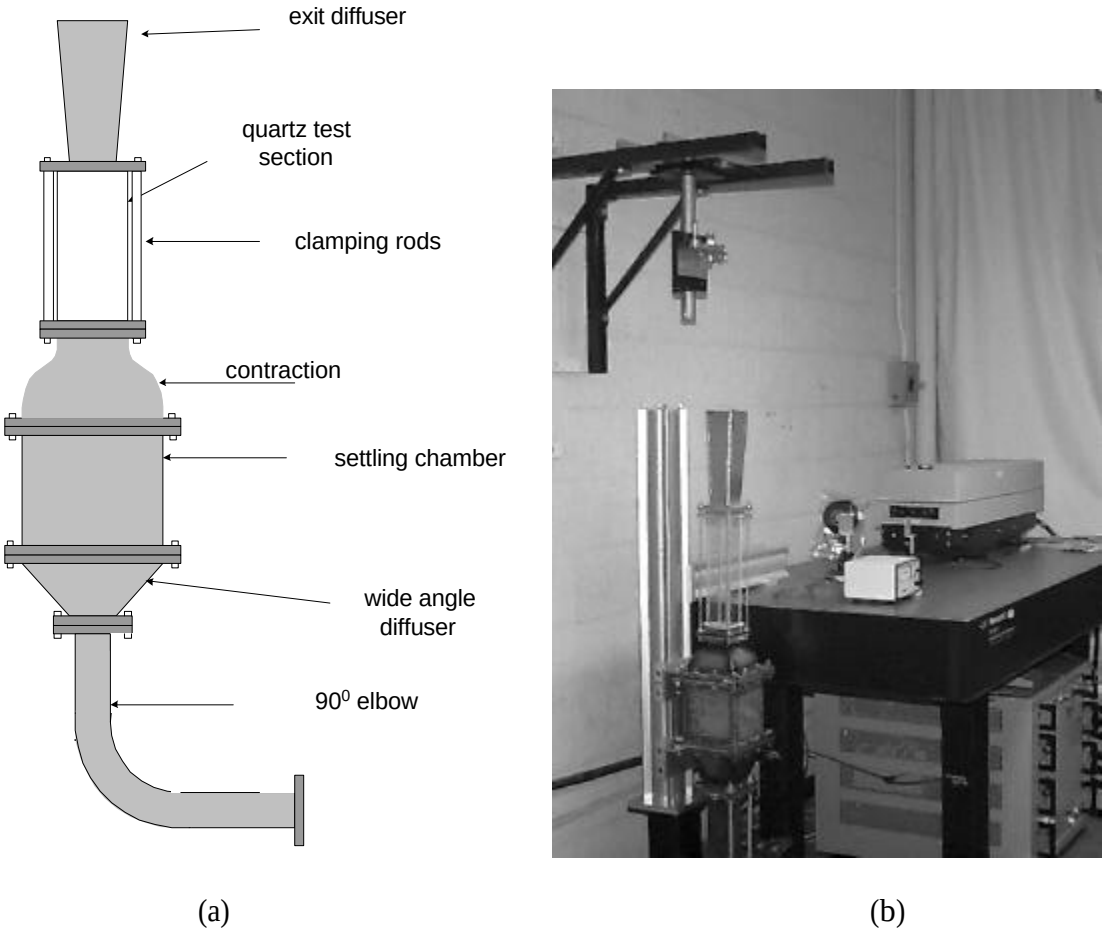

Figure 4: (a) Schematic showing the wind tunnel layout. (b) Photograph of the wind tunnel, the optical table, and the laser system.

The feeder is a capped cylinder (12 mm ID) with a tapered bottom connected to a 4-mm tube (Figure 5). Within the feeder a wire mesh was suspended; the mesh also acted as a support for a mound of particles. A jolt to the feeder resulted in particles falling through the mesh and into the feeder tube. A small air-driven piston, controlled electronically for timing purposes through a solenoid valve, glanced the side of the feeder to provide the required jolt. The mesh used inside should be larger than the finest through which the particles will pass, such that only a few hundreds of particles fell for each run. Table 3 provides a list of meshes that were used for our experiments.

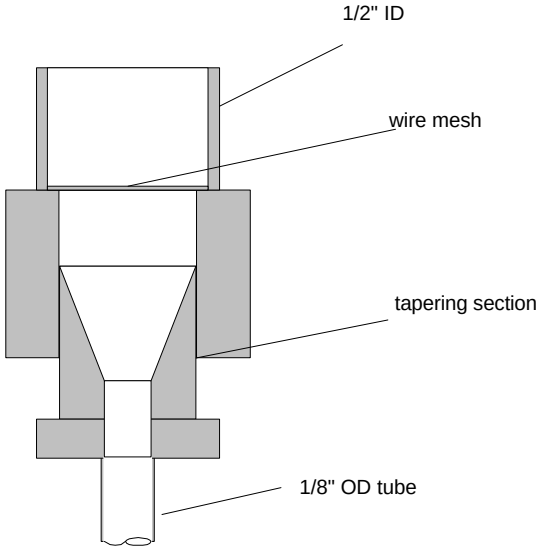

Figure 5: Cross-sectional view of the coal feeder.

Particles Size (μm)	Mesh Used in Feeder
150-180	60
125-150	70
106-125	80
63-75	100

Table 3: Particles sizes and corresponding mesh used in feeder.

E. Laser system and associated optics

The laser used was a Nd:YAG laser which operates at a pulse rate of 10 Hz and with a maximum energy of 850 mJ in the primary (1064 nm) output. The pulse duration was 100 μs. At the ignition point, the beam diameter normal to its direction of propagation was approximately 3 mm on each pass. The laser was triggered externally by a digital pulse generator; a second pulse generator was synchronized with the first to control the delay time between firing of the feeder and the laser gate, which determined the delay in the passage of the laser pulse through the test section.

The laser beam was focused through the tunnel using a convex lens (focal length 750 mm). It was defocused upon leaving the test section using a concave lens (focal length 150 mm), and folded back to the ignition point using two prisms. The use of two laser passes through the test section achieved more spatial uniformity in heating the coal particles and allowed for higher energy input than a single laser pass. The beam was finally stopped by a beam dump.

F. Experiment procedure

A typical run of our experiment is conducted as follows: The coal and oxygen concentration were first chosen for study. The coal was then loaded into the feeder. The delay time between the triggering of the feeder and the appearance of the coal sample at the feeder tube exit was visually observed and timed with a stop watch; typical values were ~2.3-2.9 s. The gas flow rate required to ensure that particles move slowly upward at the point of ignition was determined by visual observation during this time as well. The digital pulse generator was then programmed for the delay time to trigger the laser gate. Next, a laser pulse energy was set. At each laser pulse energy, 20 attempts at ignition were made in order to measure the ignition frequency or probability, which is the parameter sought from these studies. A digital storage oscilloscope recorded the signal from the detector, which determined whether or not particle(s) ignited on each attempt. The experiment

was repeated over a range of laser pulse energies to produce a laser energy versus ignition frequency plot, which we refer to as an ignition distribution. Detailed, step-by-step procedure of the conduct of each day's experiment is provided in Appendix D.

Figure 6 shows a pair of detector signals from a experimental run in which ignition did not occur. The sharp spike observed by the detectors arise from the rapid heating caused by the laser pulse, and the cooling due to radiative and convective losses from the particle surface, as we have shown previously [4]. Figure 7 shows the same two detectors observing a run in which ignition does occur. The signals are dramatically different due to the ignition and subsequent combustion. Both traces still show the initial spike, due to laser-induced heating followed by surface cooling. In this case, however, the temperature to which the particle(s) equilibrated was at or above that necessary for ignition. As we have shown previously, the particles ignite heterogeneously on the solid particle surface prior to any evident expulsion of volatile matter.

The ignition traces also show the characteristic two-pulse combustion behavior we observed previously in a similar experiment [4]. The two pulses following the initial spike were observed by high-speed video to be due to the consecutive evolution and combustion of volatile matter ejected from the particle. This combustion behavior is observed consistently in every ignited experimental run when testing with subbituminous and high-volatile bituminous coal. We hypothesized in the referenced article that the two successive pulses of volatile matters are due to the evolution of tar and oils, followed by combustible light gases (CH_4, H_2, CO). Of course, for this study, we are interested in mainly the ignition process, thus our measurements focus only on the point in time circled in Fig. 7, which corresponds to the ignition point. The measurement of the particle temperature at ignition, and its use in extracting ignition rate constants are described in sections I.G, IV, and V.

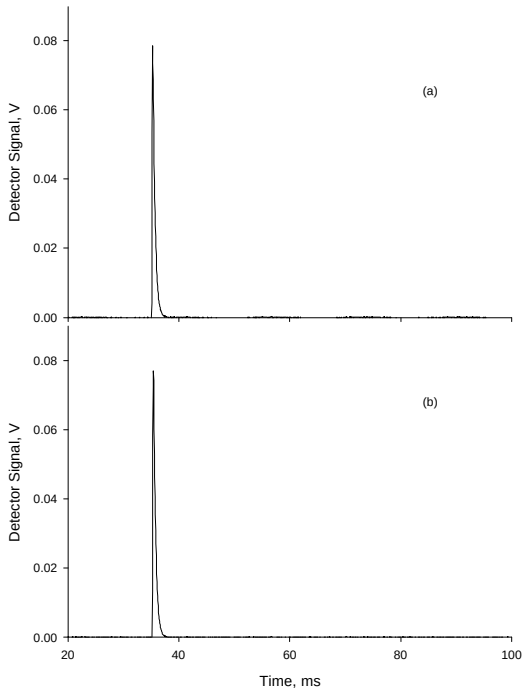

Figure 6: Detector signal traces from an ignition attempt in which ignition did not occur. (a) Signal from channel with a filter centered at wavelength 0.80 μm with bandwidth of 10 nm. (b) Filter centered at 0.656 μm with bandwidth of 40 nm.

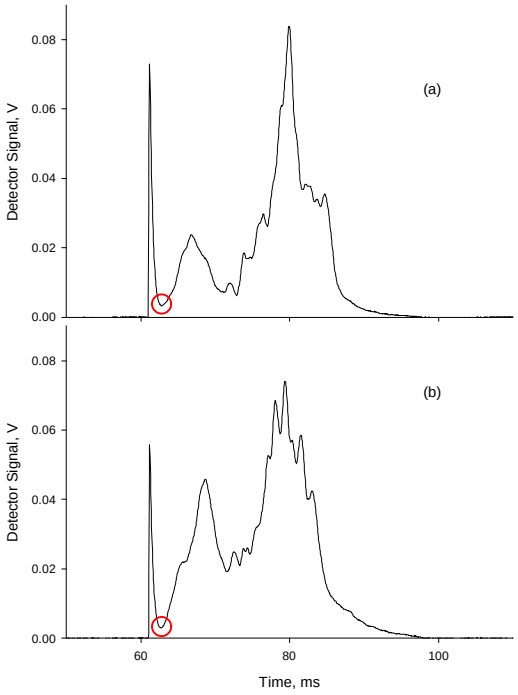

Figure 7: Detector signal traces from an experimental run in which ignition occurred. (a) and (b) have same descriptions as previous figure. The ignition point in both figures is circled.

G. Two-color pyrometry system

1. Theory of Operation

This section describes the operational principles and expected performance of a two-wavelength pyrometer used for particle-temperature measurement. The specific application in this instance is the measurement of pulverized coal temperatures *at ignition* in an experiment where one to five particles are ignited by a high-energy laser pulse. The light emitted by the igniting particles is collected by a train of optics, divided into two or three light paths via a trifurcated optical-fiber bundle, passed through a narrow bandpass interference filter, and finally detected by a photomultiplier tube (PMT). Here we will examine the expected signal levels at the pyrometer, and gauge the instrument's temperature-measurement sensitivity.

We will assume coal particles to be gray, and thus emit light according to Planck's blackbody spectral distribution, modified by its coefficient of emissivity:

$$E_\lambda(T) = \frac{\varepsilon C_1}{\lambda^5\left[\exp\left(\frac{C_2}{\lambda T}\right) - 1\right]}, \tag{1}$$

where ε is the coal emissivity, λ is the wavelength, and T is the particle temperature. C_1 and C_2 are the usual constants for Planck's spectral distribution.

A very good approximation (<1% error at all wavelengths) to Planck's distribution is:

$$E_\lambda(T) \approx \frac{\varepsilon C_1}{\lambda^5}\exp\left(\frac{-C_2}{\lambda T}\right), \tag{2}$$

and we will make use of this approximation for the remainder of this paper. The units of Eq. (1) or (2) are $\left[\frac{W}{m^2 \cdot \mu m}\right]$, since each describes the power emitted by a gray body, per surface area, within an infinitesimally small wavelength interval.

A two-wavelength, or two-color, pyrometer works on the principle that the temperature of a gray surface or a blackbody can be determined simply by measuring the light (power) emitted by that surface at two *separate but known* wavelengths. This principle is easily verified by examining Eq. (2), in which the variable, E_λ (which is measured in the experiment), is dependent on λ and on T. Thus, if E_{λ_1} and E_{λ_2}, which represent the power measured at wavelengths λ_1 and λ_2, respectively, were measured, the ratio of the powers, $E_{\lambda_1}/E_{\lambda_2}$, would yield the single unknown, T:

$$\frac{E_{\lambda 1}}{E_{\lambda 2}} = \left(\frac{\lambda_2}{\lambda_1}\right)^5 \exp\left[\frac{-C_2}{T}\left(\frac{1}{\lambda_1} - \frac{1}{\lambda_2}\right)\right]. \tag{3}$$

The importance of the assumption of blackbody or gray body (constant ε) is now obvious from examining Eq. (3), where the ratio of emissivities at the two wavelengths is assumed to be unity. The actual determination of the power emitted by the particles is complicated by the fact that various optical components lie in the path between the particle and the detector, and that the detector has variable response, depending on the wavelength of light falling on it. Nevertheless, the general principle of operation of the two-color pyrometer is as described above.

We now develop a more rigorous expression of the power detected at the PMT in order to determine the expected pyrometer performance. The *intensity* of light given off by a gray body at temperature T is:

$$I_\lambda(T) = \frac{\varepsilon C_1}{\pi\lambda^5}\exp\left(\frac{-C_2}{\lambda T}\right)\left[=\right]\frac{W}{m^2 \cdot \mu m \cdot sr}. \tag{4}$$

Note that the principal difference between Eq. (2) and (4) is that the latter is the power emitted by a gray body, per unit surface area, per infinitesimally small wavelength interval, and per infinitesimally small solid angle. These dependencies are shown schematically below.

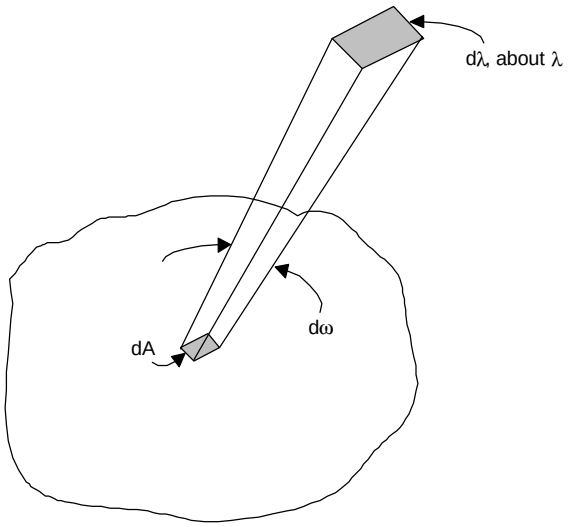

Figure 8: Schematic showing nomenclature for Planck's spectral intensity distribution.

The typical experimental set-up currently in use in our lab is shown in the figure below, assuming that only a single particle is in view (if multiple particles are present, the analysis remains the same, except for the inclusion of a multiplication factor equal to the number of particles).

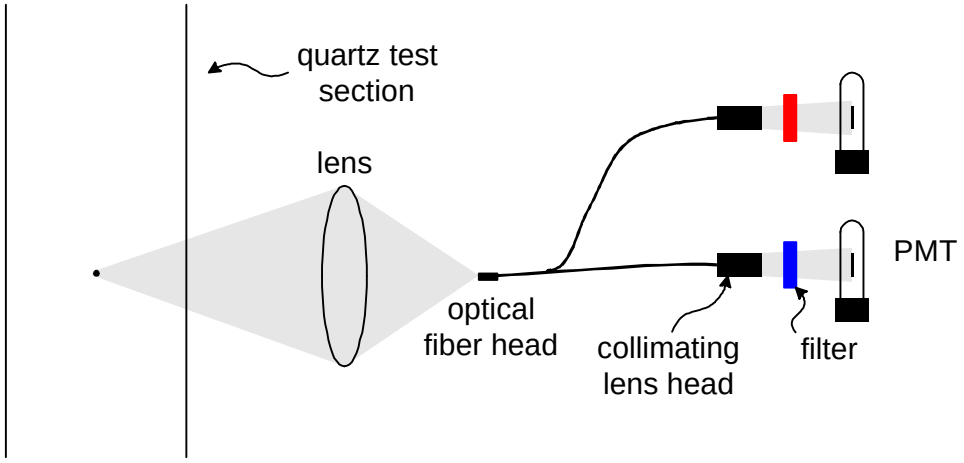

Figure 9: Layout of pyrometer set-up used for particle temperature measurement. Note that a third detection channel may be included, if desired.

Loss of light from the igniting particle occurs as the light passes through *each* optical component, and the power that finally arrives at the detection surface of each PMT is given by:

$$P = \left[\frac{\varepsilon C_1}{\pi\lambda^5}\exp\left(\frac{-C_2}{\lambda T}\right)\right][A\Omega][\Delta\lambda]\tau_{\substack{test\\section}}\tau_{lens}\tau_{\substack{optical\\fiber}}\tau_{\substack{lens\\head}}\tau_{filter}\tau_{\substack{PMT\\window}} \qquad (5)$$
$$= I_\lambda(T)\cdot A\Omega\cdot\Delta\lambda\cdot\tau_{loss}[=]\ W.$$

In words, the power that arrives at the PMT detection surface is simply the gray body's emitted intensity (I_λ), times the area-solid angle factor ($A\Omega$, or etendue), times the spectral bandwidth of the filter ($\Delta\lambda$), and finally multiplied by a factor which accounts for all the transmission losses due the optical components in the system. In the expression for P, I_λ depends on the particle temperature (which is what we seek) and the wavelength of the chosen filter, $\Delta\lambda$ depends on the optical bandwidth (FWHM) of the filter, and both the etendue and τ_{losses} depend on the optical system. Note, however, that all three factors are fixed, and do not change from run to run, so long as the optical system and filters do not change. While Eq. (5) can be used to calculate the power detected by the PMT, and can even be used to determine the particle temperature in a single-color pyrometer, the solution is highly uncertain due mainly to the uncertainties in the particle emissivity, the etendue, and the various transmission losses. This uncertainty is the reason that two-color pyrometers are more favored.

To complete this analysis, the signal (S), as an electrical current, developed by the PMT is simply:

$$S = I_\lambda(T)\cdot A\Omega\cdot\Delta\lambda\cdot\tau_{loss}\cdot R_\lambda \qquad (6)$$

where S has units of amps (A). R_λ is referred to as the PMT's *responsivity*, and has units of A/W. (The subscript on responsivity is a reminder that this value is a function of the wavelength of light that strikes it.) Input of this current into an appropriate current-to-voltage converter will then produce a voltage for detection.

Starting with Eq. (6), it is now possible to develop an expression for the ratio of two signals from a two-color pyrometer:

$$\frac{S_1}{S_2} = \left(\frac{I_{\lambda 1}}{I_{\lambda 2}}\right)\left(\frac{\Delta\lambda_1}{\Delta\lambda_2}\right)\left(\frac{\tau_{loss,1}}{\tau_{loss,2}}\right)\left(\frac{R_{\lambda 1}}{R_{\lambda 2}}\right), \tag{7}$$

where the subscripts 1 and 2 refer to the two colors or signal paths in the pyrometer. In Eq. (7), notice that while the etendue for each color divides out, the transmission loss does not, since the losess due to optical components are in general dependent on the wavelength of light (e.g. transmission loss in the optical fiber is higher for shorter wavelengths than for long wavelengths). Substituting in for the gray body intensity (Eq. (4)) and rearranging, Eq. (7) becomes:

$$\begin{aligned}\frac{S_1}{S_2} &= \left[\frac{I_{\lambda 1}}{I_{\lambda 2}}\right]\left(\frac{\Delta\lambda_1}{\Delta\lambda_2}\right)\left(\frac{\tau_{loss,1}}{\tau_{loss,2}}\right)\left(\frac{R_{\lambda 1}}{R_{\lambda 2}}\right) \\ &= \left[\left(\frac{\varepsilon_1}{\varepsilon_2}\right)\left(\frac{\lambda_2}{\lambda_1}\right)^5 \exp\left(\frac{-C_2}{T}\left(\frac{1}{\lambda_1}-\frac{1}{\lambda_2}\right)\right)\right]\left(\frac{\Delta\lambda_1}{\Delta\lambda_2}\right)\left(\frac{\tau_{loss,1}}{\tau_{loss,2}}\right)\left(\frac{R_{\lambda 1}}{R_{\lambda 2}}\right).\end{aligned} \tag{8}$$

Assuming that coal behaves as a gray body (ε does not depend on wavelength), the ratio of emissivities becomes one, and Eq. (8) can be regrouped to become:

$$\frac{S_1}{S_2} = \left(\frac{\lambda_2}{\lambda_1}\right)^5 \exp\left(\frac{-C_2}{T}\left(\frac{1}{\lambda_1}-\frac{1}{\lambda_2}\right)\right)K, \tag{9}$$

where the calibration constant, K, is defined as:

$$K \equiv \left(\frac{\Delta\lambda_1}{\Delta\lambda_2}\right)\left(\frac{\tau_{loss,1}}{\tau_{loss,2}}\right)\left(\frac{R_{\lambda 1}}{R_{\lambda 2}}\right). \tag{10}$$

K is determined using Eq. (9) by directing the pyrometer at a blackbody source whose temperature is accurately known and then measuring the signals at the two wavelengths. The measured signals are then plugged into the rearranged Eq. (9):

$$K = \left(\frac{S_1}{S_2}\right)\left(\frac{\lambda_1}{\lambda_2}\right)^5 \exp\left[\frac{C_2}{T}\left(\frac{1}{\lambda_1}-\frac{1}{\lambda_2}\right)\right]. \tag{11}$$

This calibration eliminates the need to know accurately the transmission losses, filter bandwidths, and PMT responsivities, and is the main reason that two-color pyrometers are more often used than single-color pyrometers.

Once K is determined from calibration, the pyrometer is ready for use to measure particle temperatures. Directing the pyrometer now at igniting coal particles and measuring the signals, S_1 and S_2, these values can then be substituted into the following equation, which is simply a rearrangement of Eq. (9), in order to determine the particle temperature:

$$T = \frac{-C_2\left(\frac{1}{\lambda_1} - \frac{1}{\lambda_2}\right)}{\ln\left[\frac{1}{K}\left(\frac{S_1}{S_2}\right)\left(\frac{\lambda_1}{\lambda_2}\right)^5\right]} . \qquad (12)$$

To get an idea of a two-color pyrometer's sensitivity for measuring temperatures, we can plot $\frac{S_1}{S_2}$ from Eq. (8) versus T for various pairs of filter (each with a different center wavelength and optical bandwidth), and assuming some reasonable values for the transmission losses. The responsivities used are typical wavelength-dependent values supplied by the PMT vendor. The following cases are considered:

	Filter 1		Filter 2	
	Center wavelength λ, nm	Filter bandwidth $\Delta\lambda$, μm	Center wavelength λ, nm	Filter bandwidth $\Delta\lambda$, μm
Case 1	400	10	800	10
Case 2	400	40	800	10
Case 3	600	10	700	10
Case 4	500	10	600	10
Case 5	500	40	600	10
Case 6	500	40	700	10

The results of these calculations are shown in Figure 10, where the ratio, S_1/S_2, is plotted as a function of particle temperature. The K values shown are calculated using Eq. (10) above, assuming $\tau_{loss,1}$=0.75 and $\tau_{loss,2}$=0.5, and the responsivities, R_{λ_1} and R_{λ_2}, are taken from the data sheet provided by the PMT manufacturer. These calculations are for illustrative purposes only, so the exactness of the values used is unimportant.

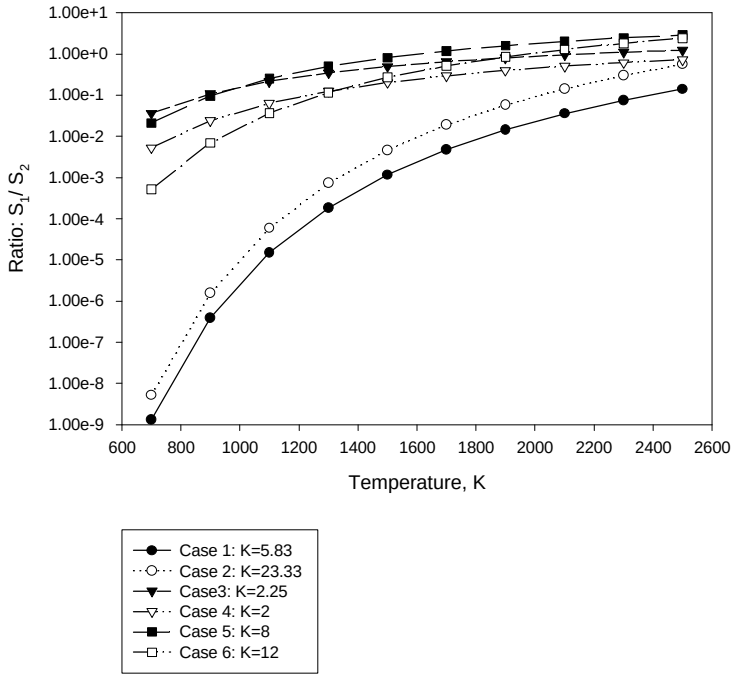

Figure 10: Plot of calculated signal ratios, S_1/S_2, versus temperature of body being observed. Case number is referenced to table above, and values of K are calculated using Eq. (10).

It can be seen in Figure 10 that the highest sensitivity to temperature, or the largest slope, $\frac{d\left(\frac{S_1}{S_2}\right)}{dT}$, occurs for cases 1 and 2, while the lowest pyrometer sensitivity in pyrometer performance occurs in cases 3, 4 and 5. It can be concluded from these calculations that the best pyrometer performance occurs when λ_1 and λ_2 are widely separated in wavelength, while the bandwidth of the filters is of secondary importance (as shown by the comparable sensitivity of cases 4 and 5). There is, however, one further consideration: At very short wavelengths, the signal may be so low (due to

the nature of Planck's blackbody distribution function and the low PMT responsivity) that it is at a level near or below the noise level. Thus, while the goal should be to maximize the separation of the two wavelengths of the filters chosen for the pyrometer, the lower wavelength is also limited by the detection limit set by the signal-to-noise ratio. These observations can be confirmed by taking the derivative of S_1/S_2 (Eq. (9)) with respect to T.

2. System Design

The layout of the pyrometry and photography system is shown in Figure 11. The receiving optics (lens and optical fiber bundle) of the pyrometer is shown to the right of the test section, and the calibration source is to the left. The path of the calibration beam is shaded in gray while the path of the light captured by the receiving optics is outlined only. The outline is present on the region between the center of the test section and the achromat lens to denote that the two lenses have been matched to capture the same solid angle. This point will be explained in detail later. The high-speed camera system is shown in its position above the receiving optics, and viewing the ignition point in the test section at an angle through a chopper wheel.

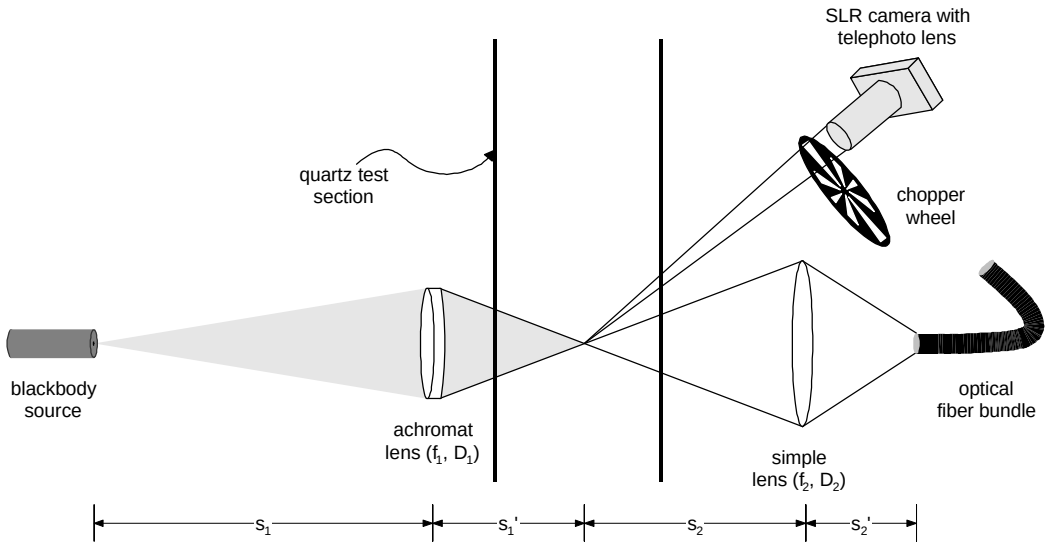

Figure 11: Schematic showing layout of pyrometry system relative to experiment, including receiving optics, calibration (blackbody) source, and high-speed photography system.

The starting point for the design of the optical system is the constraint that we will be dealing with extremely low light levels – as low as the light emitted by a single 100-μm coal particle at 500°C. Thus, the need to maximize the amount of light that is collected by the receiving, or detection, optics, drives our system design. The fiber-optic bundle can receive light input at a maximum total angle of 68°; no standard lens is this fast. Our system therefore will be limited by the "speed" of the simple lens, and we simply choose the "fastest" (lowest f/D, or focal length-to-diameter ratio) lens we can find. For our system, we've chosen an f=62.9 mm/D=50.8 mm lens, giving a f/D of 1.23.

To determine the location of the receiving lens, we consider that the diameter of the fiber-optic bundle is 5.5 mm, which is approximately one-half the diameter of the area from which we want to detect igniting particles. We make this choice even though the actual ignition point is only ~2-3 mm in diameter in order to give a margin of error for alignment and for particle motion. This choice of detection area means that we want 2:1 imaging, or a magnification of 0.5. With this constraint we can now calculate the distances s_2 and s_2' shown in Figure 11. The lens equation is:

$$\frac{1}{s_2} + \frac{1}{s_2'} = \frac{1}{f_2}, \tag{13}$$

which relates the object distance (s_2), the image distance (s_2'), and the focal length of the lens. The additional constraint is the magnification (M) of 0.5:

$$M = \frac{s_2'}{s_2} = 0.5. \tag{14}$$

Substituting Eq. 14 into Eq. 13, we find that for 2:1 imaging:

$$s_2 = 2s_2', \text{ and}$$

$$2s_2' = 3f,$$

and using f_2=62.9 mm in this case gives s_2'=94.4 mm (3.7 in.) and s_2=188.7 mm (7.4 in.).

We now move to the specification of the optics for the calibration source. Here we have two considerations: (1) the need to match the solid angle subtended by the receiving optics to the image of the calibration source, as shown in Figure 11 (that is, we want to fill the receiving lens with the light from the calibration source, just as igniting particles would); and (2) the desired demagnification of the calibration source, which is a 1-mm diameter blackbody source.

To satisfy the first consideration, we want to match the angles, α_1 and α_2, shown in Figure 12. The two lenses have different diameters, and to match the angles, we simply note the similar angles:

$$\alpha_1 = \alpha_2$$

$$\frac{s_1'}{D_1} = \frac{s_2}{D_2}$$

s_2 and D_2 are set from our previous consideration, and we choose D_1 to be 25 mm, since a fast achromat lens is much more widely available in this size than in the 50 mm version. (The need for an achromat lens is explained later.) This choice results in s_1'=92.9 mm (3.7 in.).

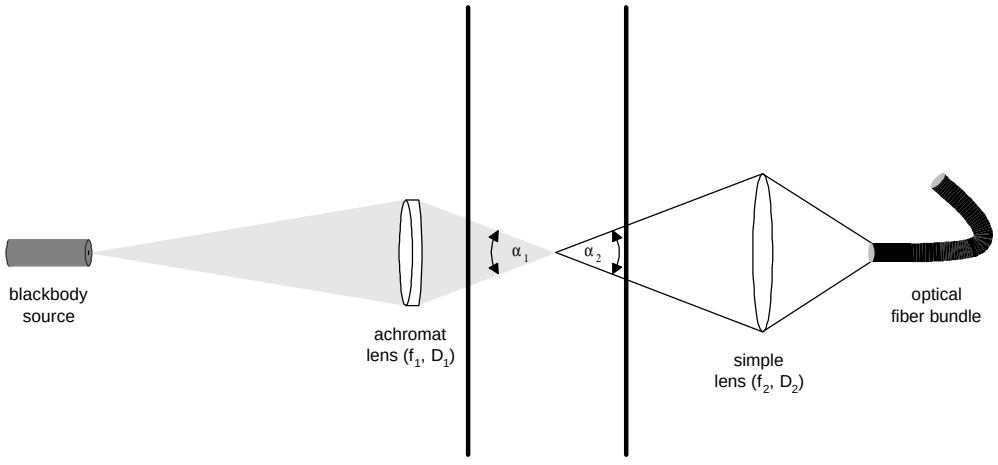

Figure 12: Schematic showing the angles subtended by the calibration-source imaging optics, and the receiving optics.

The second consideration involves the chosen demagnification of the calibration source. The coals we will use are in the size range of 60-200 μm diameter, and the blackbody source is 1 mm in

diameter. Thus, a demagnification factor of 3 to 10 (M=1/3 to 1/10) is desired to simulate the possible range of particle size and numbers we might encounter in the experiment. To specify the lenses' focal length and s_1, we again apply the lens equation and the definition of magnification:

$$M = \frac{s_1'}{s_1}$$

$$\frac{1}{s_1} + \frac{1}{s_1'} = \frac{1}{f_1}$$

These two equations can be solved simultaneously for the two unknowns, s_1 and f_1; the solutions are shown in Table 4.

s_1' = 92.9

M	f_1	f_1 (in.)	s_1	s_1 (in.)
0.333333	69.7	2.7	278.7	11.0
0.25	74.3	2.9	371.6	14.6
0.2	77.4	3.0	464.5	18.3
0.166667	79.6	3.1	557.4	21.9
0.142857	81.3	3.2	650.3	25.6
0.125	82.6	3.3	743.2	29.3
0.111111	83.6	3.3	836.1	32.9
0.1	84.5	3.3	929.0	36.6

Table 4: Calculation of focal length, f_1, and image distance, s_1, for the calibration source. All units are in mm unless noted otherwise.

Our final lens selection for the calibration source is dictated by the available achromat lenses, and the reasonableness of the required s_1, which is excessive in some instances. An f=75 mm achromat lens is available, so our calibration optics will have these final characteristics:

D_1 = 25 mm

f_1 = 75 mm

s_1' = 92.9 mm (3.7 in.)

s_1 = 389.2 mm (15.3 in.)

M = 1/4.2

The 1-mm diameter calibration source will be projected into the test section to an image size of 238 μm (1 mm/4.2).

One final note regarding the use of an achromat lens for the calibration source. We need to project an *exact* image of the object (the blackbody) into the test section, as if the blackbody itself was placed inside, with all its colors focused to the same point. This eliminates the need to remove the test section each time we wish to calibrate the pyrometer. Simple lenses do not focus all colors of light to the same point because the refractive index of any material is a function of the wavelength of light. This is shown schematically in Figure 13. Achromat lenses are an attempt at correcting this problem, known as 'chromatic aberration', by cementing two elements of different refractive indexes together, which results in the total elimination of chromatic aberrations *at two wavelengths*, usually a blue and a red. Aberrations for the wavelengths between these are small, though not completely eliminated.

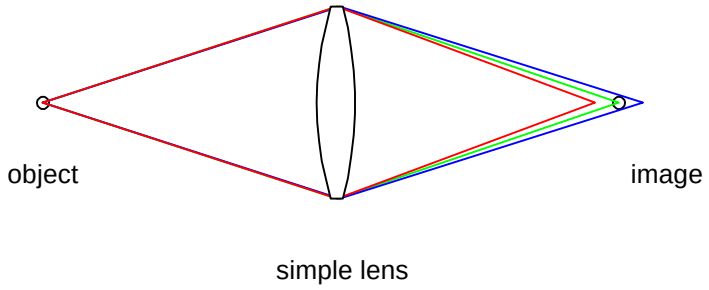

Figure 13: Schematic showing chromatic aberration caused by a simple lens.

The final component of the optical detection system is the high-speed camera. A conventional 35-mm SLR (single lens reflex) camera fitted with a 105-mm zoom lens is used. To achieve a higher magnification, a 25-mm extension tube is inserted between the lens and the camera

body. The camera is operated in the manual mode with the shutter held open and all room lighting eliminated. The light emitted by the igniting and burning particles will thus be captured. To produce discrete images on the high-sensitivity black-and-white film, a chopper wheel is placed in front of the camera lens to provide 'shuttering' at approximate 500 Hz. Thus, one image will be recorded roughly every 2 ms of experiment time until the igniting particles leave the camera's field of view.

3. Calibration Procedure

The goal of the calibration is to determine the calibration constant, K, of Eq. (10). Since it is not practicable to measure each variable of Eq. (10), it is simpler and more straightforward to measure this parameter by directing the pyrometer at a blackbody source whose temperature is accurately known and then measuring the signals at the two wavelengths for various temperatures. The measured signals are then substituted into Eq. (11) and K is found by a 'best fit' through the data points.

This calibration eliminates the need to know accurately the transmission losses, filter bandwidths, and PMT responsivities, and is the main reason that two-color pyrometers are more often used than single-color pyrometers. Furthermore, it should be noted the although measurements of PMT signal are made at several temperatures, the pyrometer actually requires only a single-point calibration, which means the procedure is both fast and simple.

II. Data Reduction Methodology

The measured particle temperatures at ignition is analyzed to extract the ignition rate constant by application of the Distributed Activation Energy Model of Ignition (DAEMI), which we first developed to interpret results from conventional, drop-tube, ignition experiments (see description

below and the reprint of the publication in Appendix A). The model has been modified from its original form for application to this project as described below.

Numerous experiments have been conducted over the past three decades to measure the ignition rates of pulverized coals. Most of these are reviewed by Essenhigh et al. [1], and the most popular method is described next. In order to extract rate constants from any ignition experiment, it is necessary to apply a model of the ignition process to analyze the data, which usually consists of some readily measurable parameter such as the gas temperature necessary to cause ignition. What all previous experiments have in common is that within each model, ignition is represented by a *single Arrhenius rate constant*, which of course represents some *average value* for the coal particles within that sample. This method is chosen for convenience but does not accurately represent the reality, since it is well established – from single particle experiments [2] – that for coals of the same type and size, particle-to-particle variations exist. These variations include size, density, mineral-matter content, specific heat and, most importantly, chemical reactivity. Thus, our goal in this phase of study is to develop a model of coal ignition which accounts for the variation in reactivity, and to apply it to our data in order to extract more meaningful ignition rate constants.

Recently, we presented a model of heterogeneous coal ignition which accounts for particle-to-particle variation in reactivity within a sample, and showed that it correctly depicts, for the first time, all key observations from conventional drop-tube furnace experiments [3]. The Distributed Activation Energy Model of Ignition (DAEMI) accounts for the variation in reactivity by including a single preexponential factor, as usual, and a Gaussian distribution of activation energies among the particles to describe their ignition kinetics. This distribution provides the particle-to-particle variation in reactivity we seek to inject into our model. By adjusting the parameters in the model, main characteristics of experimental results were captured, namely (1) the gradual increase in

ignition frequency with increasing gas temperature, and (2) the variation of the slope of the ignition frequency with oxygen concentration.

The DAEMI models the conventional ignition experiment by allowing for the particles within the coal sample to have a distribution of reactivity, rather than a single average value. We prescribe that all the particles have the same properties, including the preexponential factor in the Arrhenius rate constant describing their ignition reactivity, and that their activation energy is distributed according to the Gaussian (or normal) distribution:

$$f(E) = \frac{1}{(2\pi\sigma^2)^{0.5}} \exp\left[\frac{-(E-E_o)^2}{2\sigma^2}\right] \tag{15}$$

where Eo is the mean and σ is the standard deviation of the distribution. The expression

$$\int_{E}^{E+\Delta E} f(E)\, dE \tag{16}$$

describes the frequency or probability that particles within a sample have an activation energy in the range E to E+ΔE.

The DAEMI divides a prescribed distribution into discrete energy intervals of $\Delta E = 1$ kJ/mol, and considers only the energy range of E_o-3σ to E_o+3σ, rather than -∞ to +∞. The latter simplification still covers 99.73% of the distribution. The model then calculates the frequency of being in each of these intervals by numerically integrating Eq. (16) for each of the intervals.

A conventional, drop-tube, ignition experiment is modeled by assuming that 10^5 particles are in the initial sample, and that they are distributed among the various ΔE intervals according to the calculated frequency of each interval. Each simulation of an experimental run under a given set of conditions is conducted on a batch of 100 randomly selected particles from the sample, keeping in mind that no particle can be selected more than once. Whether or not ignition occurs for a run is determined by the particle in the batch with the lowest activation energy, which is equivalent to

being the most reactive particle. If this particle's reactivity equals or exceeds that determined by the critical ignition condition, the batch is defined to be ignited. This is consistent with our observation [4] that single-particle ignition is discernible to the eye. This procedure is repeated 20 times at each condition, just as in actual experiments, to determine an ignition frequency at this condition. Finally, the gas temperature is varied several times and, each time, 20 runs are conducted.

Figure 14 shows an application of the DAEMI in modeling the ignition experiments of Zhang et al. [5]. Linear regressions of the experimental data are shown in the figure as solid lines, and the data points are from the model. Notice that the model correctly depicts the increase in ignition frequency with increasing gas temperature (T_g), and it captures both the decrease in the slope of the ignition frequency with decreasing oxygen concentration and the slow rate of the slope's decrease until very low oxygen concentrations. These results represent the first time that a model has depicted ignition data with such accuracy.

The original DAEMI is modified for the present experiment as follows. The initial batch of coal is assumed to contain 4×10^5 particles; this number is arrived at by determining the approximate weight of a sample and making an estimate of the number of particles assuming a spherical particle of the average size. 1300 particles are then selected randomly and act as feed into the test section; again, this number is arrived at by measurement and estimation. Three particles are further selected randomly from these 1300 to be heated by the laser pulse, keeping in mind that no particle can be selected twice.

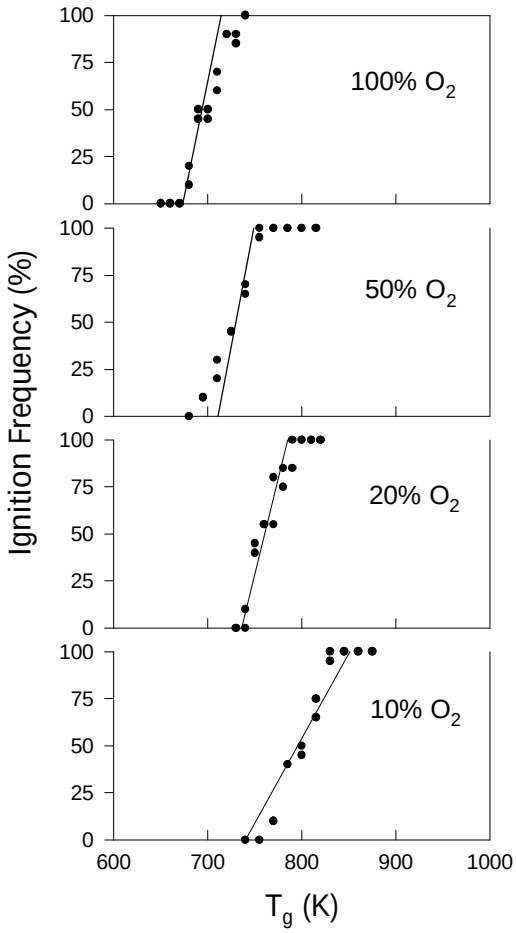

Figure 14: Linear regressions of experimental data from Ref. [5] (shown as solid lines), showing the effect of free-stream oxygen concentration on ignition of a high-volatile bituminous coal of 75-90 μm in diameter. The data points represent results from the DAEMI.

The heat generated, per unit surface are (S), by a spherical carbon particle undergoing oxidation on its external surface may be given by the kinetic expression:

$$\frac{H_G}{S} = h_c p_{O_2}^n A_i \exp\left(\frac{-E}{RT_p}\right) \tag{17}$$

Similarly, the heat loss from the surface of a particle at temperature T_p is the sum of losses due to convection and radiation. Thus, heat loss from the surface may be given as:

$$\frac{H_L}{S} = h\left(T_p - T_g\right) + \varepsilon\sigma_b\left(T_p^4 - T_g^4\right) \tag{18}$$

At the non-critical condition of ignition (as is applicable to our experiment), the following condition is satisfied:

$$H_G > H_L \tag{19}$$

Thus, equating H_G and H_L and solving for E from Eq. (17) (assuming Nu=2 as is appropriate for very small particles), we obtain [3]:

$$E = -RT_p \ln\left(\frac{\left(\frac{2k_g}{d_p}\right)(T_p - T_g) + \varepsilon\sigma_b\left(T_p^4 - T_g^4\right)}{h_c p_g^n A_o}\right) \tag{20}$$

where the required parameters for this equation were calculated as follows:

1. T_p is determined by direct measurement from the two-color pyrometer, as described in the previously in section I.G.
2. k_g, the gas thermal conductivity in the boundary layer around a heated particle is given by a linear fit to the conductivity of air determined at the average temperature of the particle surface and gas:

$$k_g = 7.0 \times 10^5\left(\frac{T_p + T_g}{2}\right) \tag{21}$$

3. A_o, the preexponential factor was arbitrarily chosen as 250 kg m^{-2} s^{-1}.
4. n, the reaction order is assumed to be 1.
5. ε, the emissivity of coal particles is chosen to be 0.8
6. h_c is defined by the equation

$$h_c = \frac{y}{y+1} H'_{C,CO} + \frac{1}{y+1} H'_{C,CO_2} \tag{22}$$

where $y = \frac{mol\ CO}{mol\ CO_2}$ was obtained from the equation [3]:

$$\frac{\text{molCO}}{\text{molCO}_2} = 59.95\exp\left(\frac{-3214}{T_p}\right) \tag{23}$$

$H'_{C,CO}$ and H'_{C,CO_2} are the heats of combustion corresponding to the following oxidation reactions:

$$\begin{aligned} C + \frac{1}{2}O_2 &\rightarrow CO; H'_{C,CO} = 9{,}210\ \frac{kJ}{kg\,C} \\ C + O_2 &\rightarrow CO_2; H'_{C,CO_2} = 32{,}790\ \frac{kJ}{kg\,C} \end{aligned} \tag{24}$$

Twenty runs were made at each laser energy to obtain ignition-frequency distributions. Detailed simulation results are provided in the following section. Although it was assumed that pulverized-coal ignition occurs heterogeneously without influence from any volatile matter that may be present, and even though the results closely fit the experimental data, DAEMI does not confirm that ignition is purely a heterogeneous process. Very few models of homogeneous ignition have been developed, and none have been tested against the available experimental data because of the inherent difficulty and uncertainty in modeling devolatilization and the combined solid-gas and gas-gas reactions.

III. Ignition-Frequency Distribution Data

The present study provides ignition frequency as a function of oxygen concentration, particle diameter and coal type. We have examined three sizes of four coals under three oxygen concentrations. At each set of conditions (coal type, size and oxygen concentration), the ignition frequency was measured over a range of laser pulse energy values. Twenty attempts at ignition were made at each laser pulse energy to determine the frequency, or probability, of ignition. The frequency thus obtained was mapped against the corresponding laser energies for these coals as

ignition-frequency distributions, and are presented below organized by coal type. The experimental data has been provided in tabular numerical format in Appendix D.

Pittsburgh # 8 – high-volatile A bituminous

Figure 15 shows the ignition-frequency distributions for the 165 μm (150-180 μm range) high-volatile A bituminous Pittsburgh #8 coal at various oxygen concentrations. It can be seen that at each oxygen concentration, the ignition frequency increases approximately linearly over a range of laser pulse energy. At each oxygen concentration, there is a lower laser energy below which the probability of ignition is zero, and a higher energy above which there is 100% ignition probability. The slope in frequency distribution is indicative of the variation of reactivity among the particles, as described in the previous section on data reduction using the DAEMI.

The ignition frequency increases with increasing laser pulse energy since high pulse energy translates to a higher particle temperature achieved. Thus, using the laser pulse to heat several randomly chosen particles from the batch of particles dropped into the experiment, there is an increasing probability that one of the heated particles will ignite as the particles are heated to higher temperatures.

The shifting of the distributions to higher laser energies as oxygen concentration is decreased is expected, since at lower oxygen levels, the amount of heat generated by the particle is decreased (see Eq. (17)). Thus, in order to achieve a constant ignition frequency as oxygen concentration is decreased, the particles must be heated initially to a higher temperature using higher laser energy.

The general observations described above applies to Figure 16 for the 116 μm Pittsburgh coal, as well as to all coals studied under all conditions. The solid and open circles in Figure 16 represent the ignition frequencies obtained for 116 μm Pittsburgh coal at 100% oxygen concentration on two different days. It can be seen that the data show excellent repeatability.

Figure 17 shows the ignition-frequency distribution for the 69 μm Pittsburgh coal. It is interesting to compare the ignition behavior for the same coal, but of different sizes. The figures for the Pittsburgh show that, as particle size is decreased, the range of laser energy needed to span 0 to 100% ignition frequency becomes narrower; i.e. the slope of the ignition distribution at a given oxygen concentration is more vertical. Furthermore, as oxygen concentration is decreased, there is a marked difference in its influence on the distributions. The smaller particles show small variation in the distributions' slope as well as smaller shifts to higher laser energy, while both these effects become pronounced for the largest coal examined.

We did not take such detailed data for a large variety of coals, so it is difficult to generalize the behavior described above to all coals. Furthermore, the complicated ignition behavior described above shows the importance of a detailed and accurate model for the interpretation of the results.

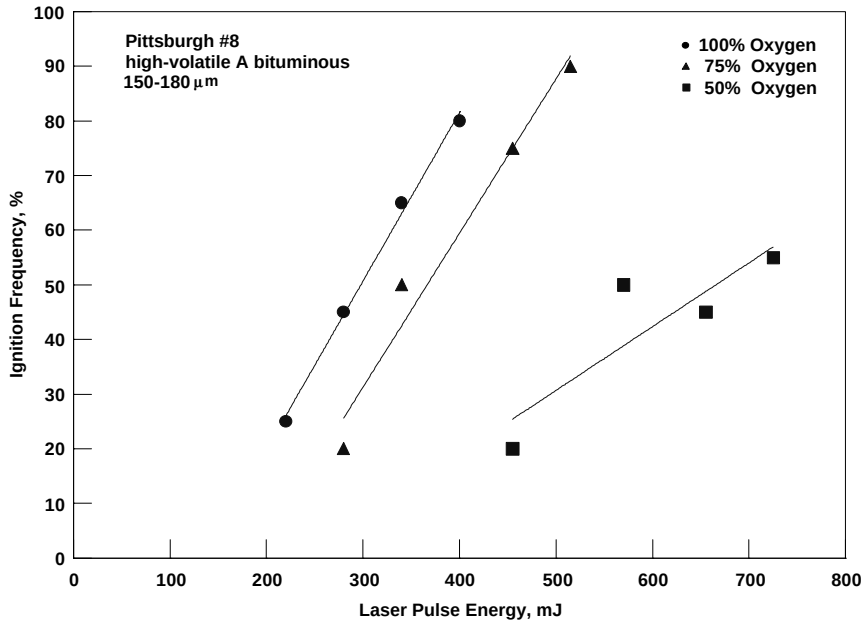

Figure 15: Ignition-frequency distribution for Pittsburgh #8 coal. Experiment conditions provided in figure legend. Lines shown are linear-regression fits.

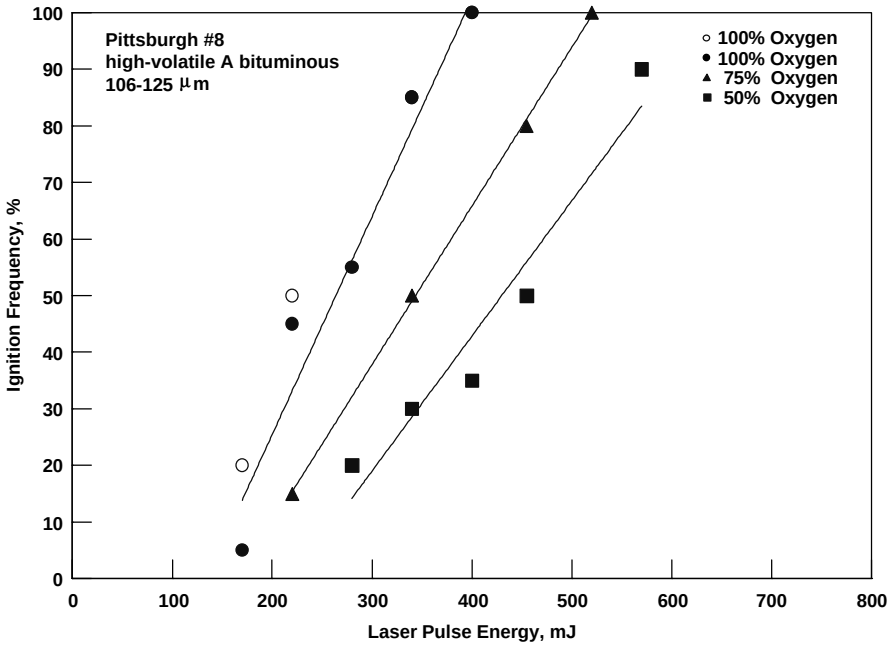

Figure 16: Ignition-frequency distribution for Pittsburgh #8 coal. Experiment conditions provided in figure legend. Lines shown are linear-regression fits.

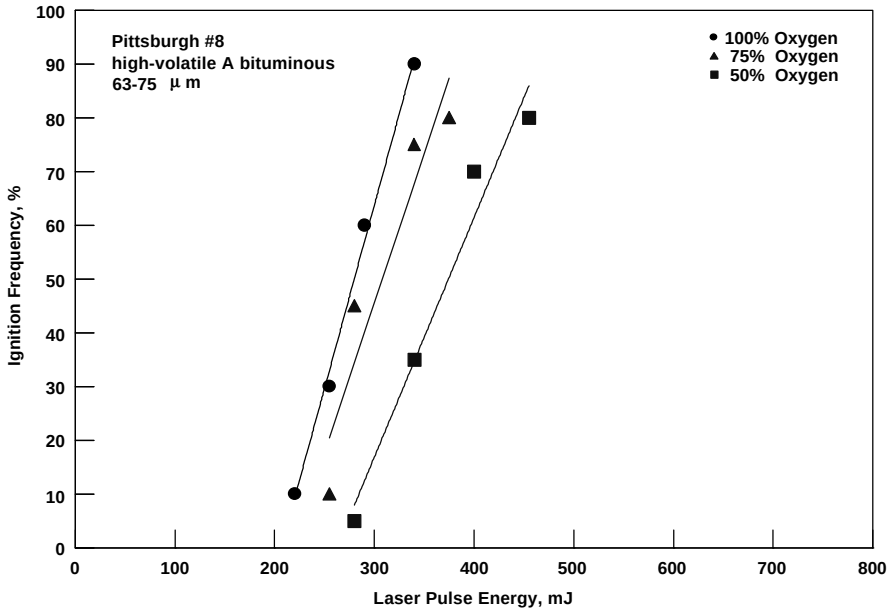

Figure 17: Ignition-frequency distribution for Pittsburgh #8 coal. Experiment conditions provided in figure legend. Lines shown are linear-regression fits.

Sewell – medium volatile bituminous

Limited ignition-frequency data for the Sewell medium-volatile bituminous coal is shown in Figure 18. Generally, the ignition behavior of this coal is dramatically different from the Pittsburgh coal, under otherwise identical experimental conditions (see Figure 16). It can be observed that Sewell reaches 100% ignition frequency over a small range of laser energy compared to the Pittsburgh #8 for a 116 μm particle at 100% oxygen concentration. Also, a change in oxygen concentration changes the slope of the frequency distribution drastically for the Sewell coal compared to Pittsburgh #8. These observations are no doubt due to the variability in reactivity distributions of the two coals.

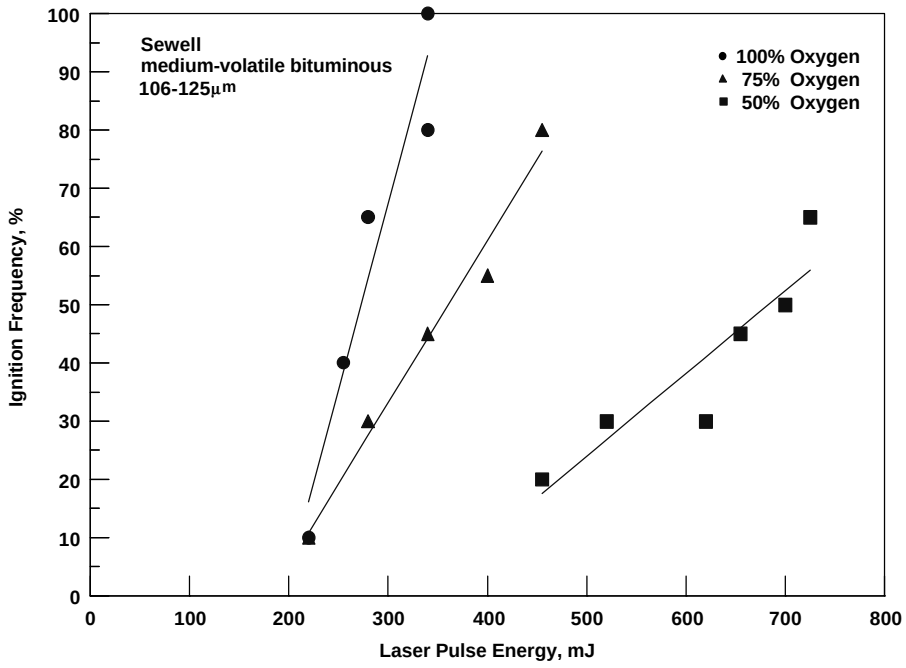

Figure 18: Ignition-frequency distribution for Sewell coal. Experiment conditions provided in figure legend. Lines shown are linear-regression fits.

Wyodak – subbituminous

Ignition distribution data for the Wyodak subbituminous coal are shown in the following series of three figures. The data is somewhat limited in oxygen-concentration coverage, but generally show wide differences from the other two coals, even though the general observations are still applicable. Again, the specific differences are no doubt due to variations in the reactivity distributions of the coals.

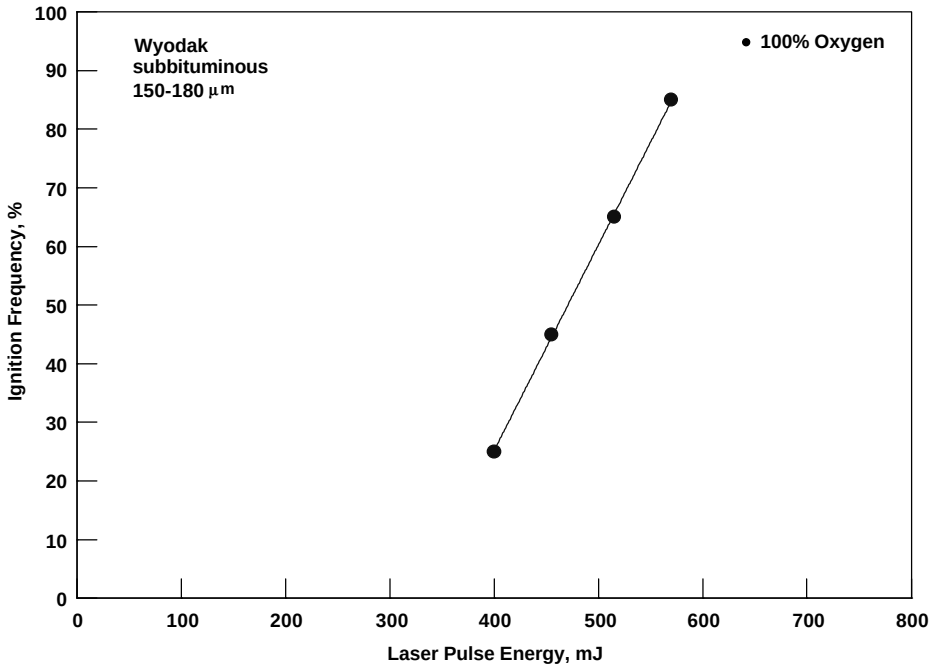

Figure 19: Ignition-frequency distribution for Wyodak coal. Experiment conditions provided in figure legend. Lines shown are linear-regression fits.

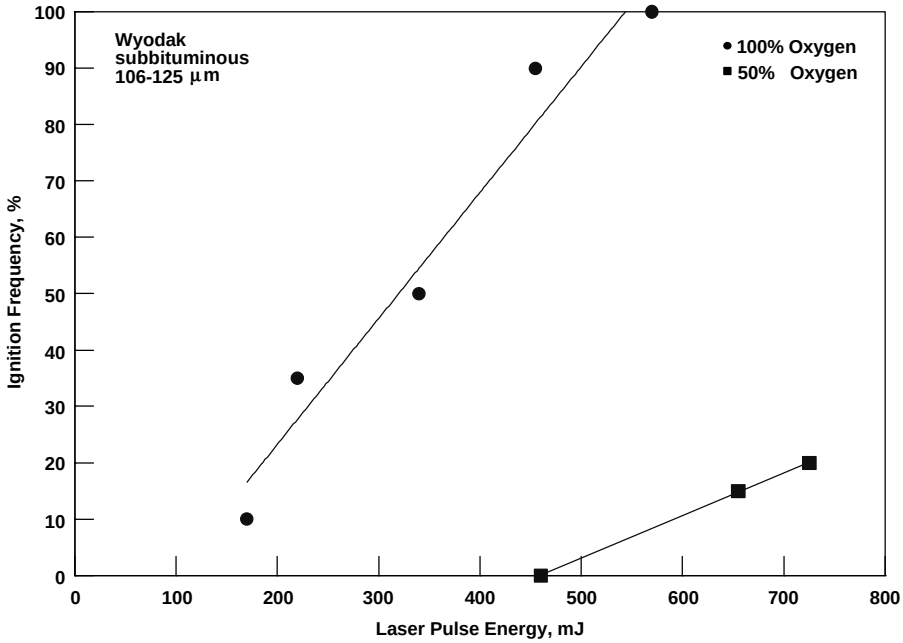

Figure 20: Ignition-frequency distribution for Wyodak coal. Experiment conditions provided in figure legend. Lines shown are linear-regression fits.

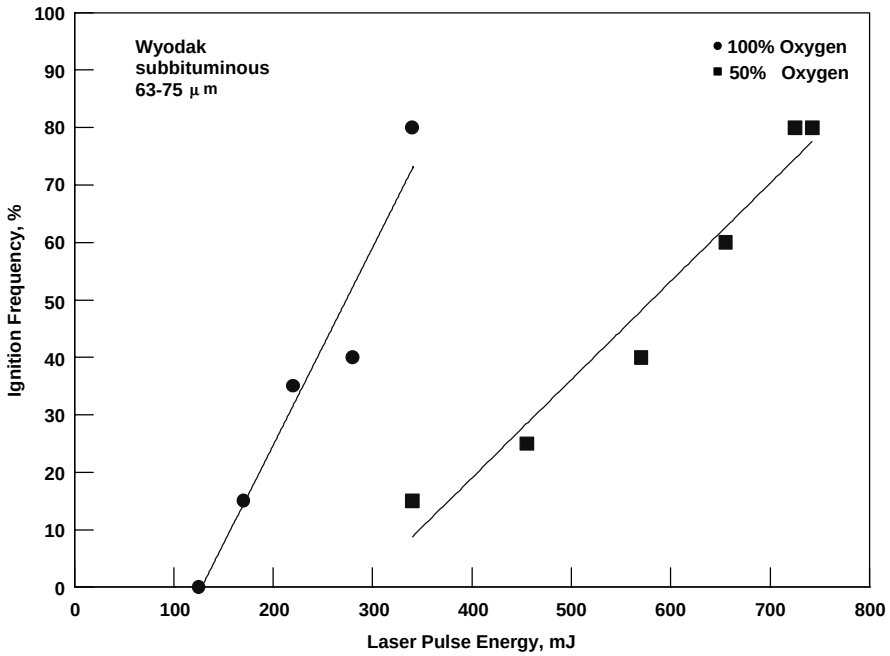

Figure 21: Ignition-frequency distribution for Wyodak coal. Experiment conditions provided in figure legend. Lines shown are linear-regression fits.

Illinois #6 – high-volatile C bituminous

Limited ignition-frequency data for the Illinois #6, high-volatile C bituminous coal is shown in Figure 22. The behavior is dramatically different from the Pittsburgh high-volatile A bituminous coal (see Figure 16) under similar experimental conditions. The differences include the slope of the distribution at 100% oxygen concentration, as well as the shift to higher laser energy and slope change when oxygen is decreased. The data shows that, even for coals of the same rank and similar elemental make-up, ignition behavior can be quite varied.

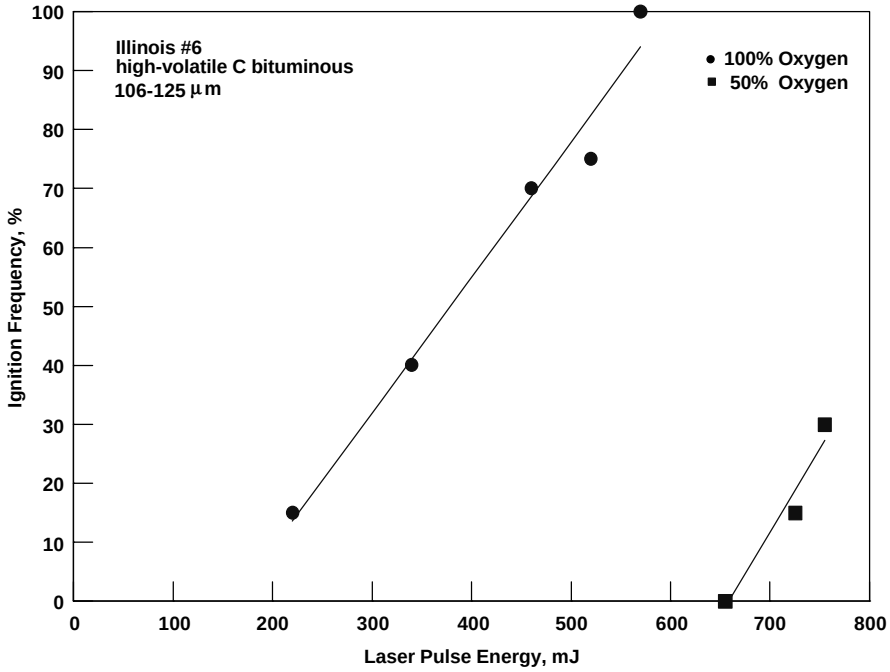

Figure 22: Ignition-frequency distribution for Illinois #6 coal. Experiment conditions provided in figure legend. Lines shown are linear-regression fits.

IV. Temperature Measurements

We have temperature measurements on a limited number of experiments, using one particular coal of one size. The Pittsburgh #8 (DECS-23), high-volatile A bituminous coal of size range 125-150 μm in diameter was chosen for this work. Our choice was dictated mainly by our

realization that (1) a large amount of sample was needed to diagnose and troubleshoot our pyrometry system, (2) the coal must be of relatively large size for ease of signal detection (high signal-to-noise ratio), (3) an extensive database of ignition frequency is available, and (4) the coal must have a relatively high reactivity for this first set of measurements. This particular coal (herein after referred to as the Base Coal) fits these criteria.

The ignition-frequency distribution of this coal is shown in Fig. 23. We have taken these data on multiple days, and have confidence in their accuracy and precision with our experiment. The data is consistent with those presented previously for this coal of both smaller and larger sizes.

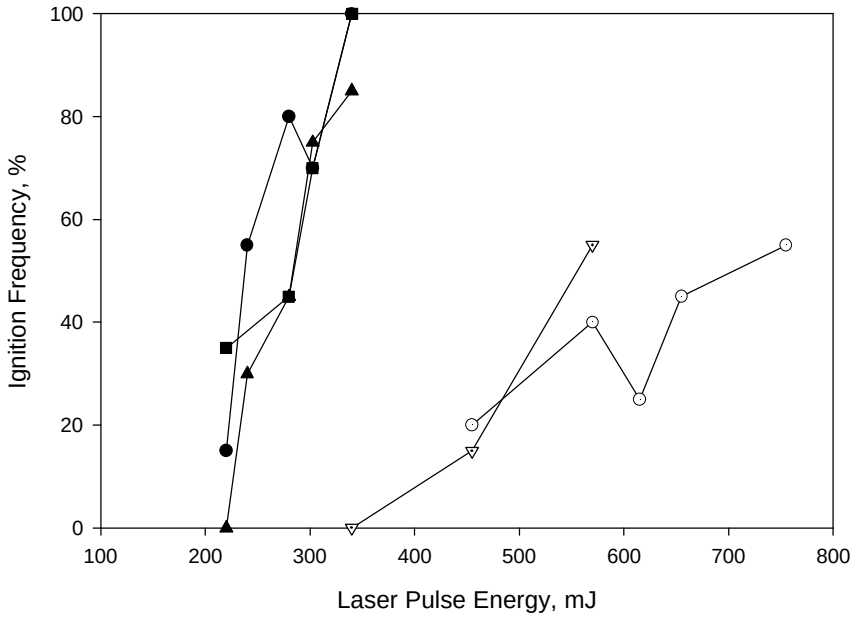

Figure 23: Ignition-frequency distribution of Pittsburgh #8 (DECS-23) coal, 125-150 μm diameter. Solid symbols are data taken at 100% oxygen concentration, and open symbols are data for 50% oxygen concentration.

Figures 24 and 25 show data from ignition experiments of the Base Coal, both at a laser energy equivalent to an ignition frequency of 50%. Figure 24 is taken at an oxygen concentration of 100%, while Fig. 25 is at 50% oxygen concentration. The same pyrometry system set-up was used

in both cases, with one channel at a center wavelength of 0.80 μm and bandwidth of 10 nm, and the other at a center wavelength of 0.655 μm and bandwidth of 40 nm.

Contrasting the difference between the two data sets, it is apparent from the raw detector signals ((a) and (b) of both Figures) that the signal for the data taken at 100% oxygen concentration is much higher than that at 50% oxygen. This might suggest that the particle temperature is much higher in the former case, as is intuitively expected since a higher oxygen level would result in higher reaction rate, and hence higher temperature, at the particle surface. However, it must be remembered that it is possible for the number of particles ignited to vary from run to run, and there is some particle size distribution present, both being factors which may influence the signal level.

The ratio of the two detector signals is shown in (c) of both figures. Note that for both channels of the pyrometer, only signals above three bits of the data-acquisition's analog-to-digital (A/D) converter are considered to be significant, i.e. non-zero. For our 16-bit A/D converter, this means that any signal below 91 μV is considered to be zero, and the ratio of the signals for this case is set to one. It is apparent from Figs. 24(c) and 25(c) that, at the ignition point, the signals are strong and non-zero.

The signal ratios are converted to temperatures, as described previously in section I.G, and presented in (d) of Figs. 24 and 25. They show that, indeed, the temperature of the 100% oxygen case (Fig. 24) is in general higher than the 50% oxygen case. It should be noted, however, that only temperatures measured in the absence of any gas-phase reactions is deemed to be a reliable measure of *particle* temperature, since it is well known that gas-phase reactions and the presence of soot will distort the pyrometry signals. At the ignition point, we have confirmed by high-speed phototgraphy that only heterogeneous reaction is occurring.

For the 100% oxygen case, the ignition temperature is found to be 1310 K, while for the 50% case, the ignition temperature is found to be 1460 K. The ignition temperature is higher for the latter case due to the higher laser energy required to reach 50% ignition frequency at the lower oxygen level. We found a distribution in the ignition temperature measured at each experimental condition; this is no doubt due to the variations in reactivity and perhaps size among the particle sample. We learned from these first measurements that it will be essential to take data for a large number of runs at each condition in order to build up meaningful statistics for data interpretation.

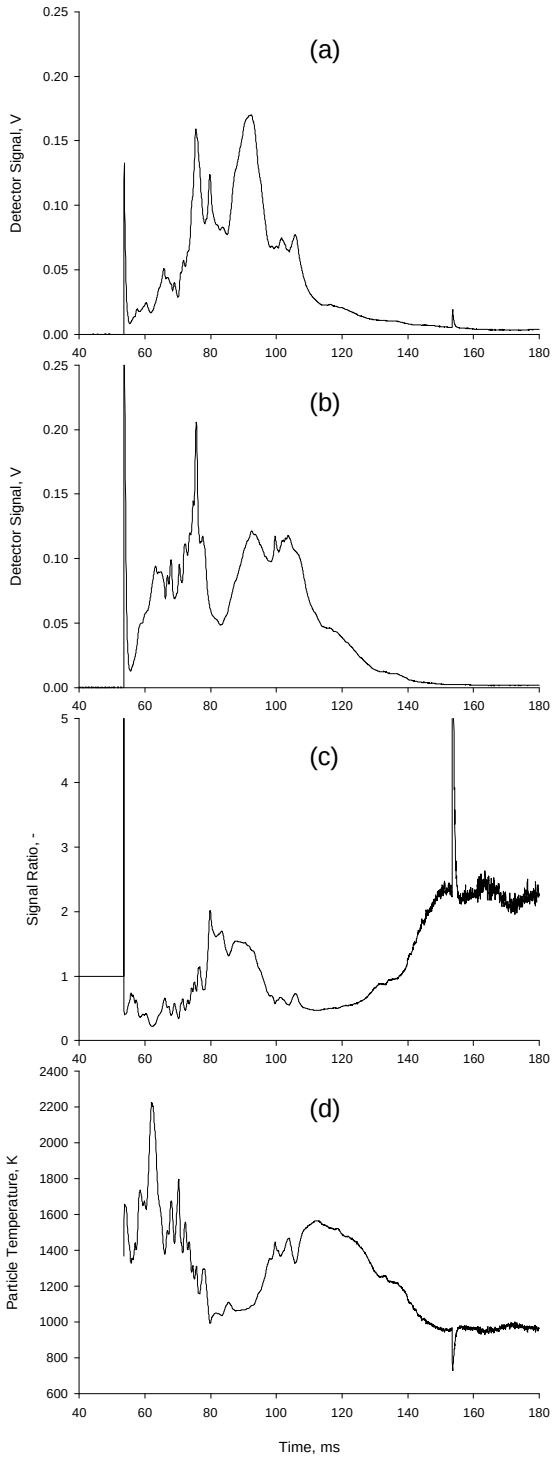

Figure 24: Data taken for particle temperature measurement. Experimental conditions for the Base Coal are 100% oxygen and laser pulse energy of 290 mJ. (a) Detector signal in channel with filter at 0.80 μm center wavelength and 10 nm bandwidth. (b) Detector signal in channel with filter at 0.656 μm center wavelength and 40 nm bandwidth. (c) Signal ratio (a):(b). (d) Interpreted temperature from (c).

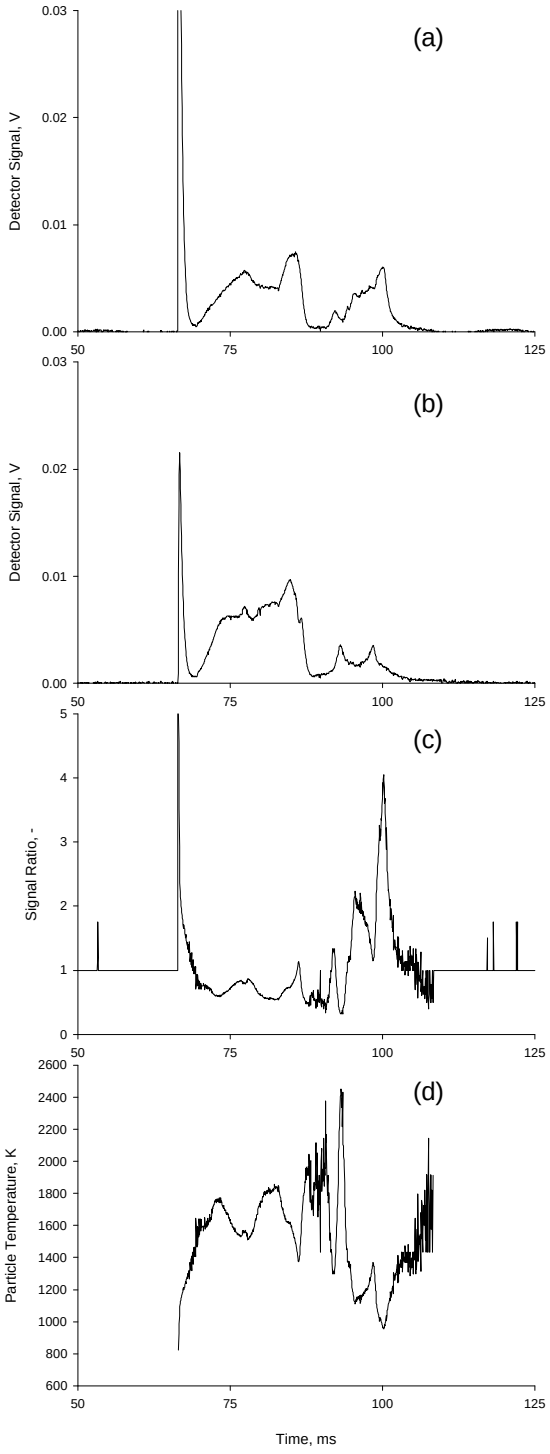

Figure 25: Data taken for particle temperature measurement. Experimental conditions for the Base Coal are 50% oxygen and laser pulse energy of 730 mJ. Figure descriptions are same as for Fig. 24.

V. Ignition-Rate Data

The interpretation of the temperature measurements shown in the previous section is made difficult by the existence of ignition temperature variations from run to run, even under otherwise identical experimental conditions. We currently have no means to deal with this finding to extract rate constants from our data. The problem is further hampered by two factors: (1) We need to make extensive measurements of ignition temperature at each condition in order to build up a large database of ignition-temperature statistics, and (2) we need to develop a means to extend our data-interpretation tool, the Distributed Activation Energy Model of Ignition, to handle our experimental findings.

Currently, we can only extract the ignition rate constant for the Pittsburgh #8 coal by using the limited ignition temperatures presented above in conjunction with simplifying assumptions regarding the expected ignition behavior with oxygen and size variations. By assuming a reaction order, n, of 1, and a preexponential factor of 500 $kg/(m^2s)$, we find the ignition rate constant distribution to have an average activation energy of 73 kJ/mol, with a standard deviation, σ, of 3.7 kJ/mol.

Conclusions

We established a novel experiment to study the ignition of pulverized coals under conditions relevant to utility boilers. Specifically, we determined the ignition mechanism of pulverized-coal particles under various conditions of particle size, coal type, and freestream oxygen concentration. We also measured the ignition rate constant of a Pittsburgh #8 high-volatile bituminous coal by direct measurement of the particle temperature at ignition, and incorporating this measurement into a mathematical model for the ignition process.

The ignition mechanism of pulverized coals in this experiment, under all conditions examined, was determined by high-speed photography to be *heterogeneous*. That is, ignition of the particles always occurred on the solid surface, prior to the evolution of volatile matter from the particles into the gas phase. This finding was most likely due to the high heating rates achieved ($>10^5$) by the laser heating, which causes the particle temperature to rise above that necessary for ignition before appreciable devolatilization occurred.

Particle temperature at ignition was measured for one size group (125-150 μm) of one coal (Pittsburgh #8, high-volatile bituminous) under two oxygen concentrations. At 100% oxygen, the ignition temperature of this coal was found to be 1310 K, while at 50% oxygen the ignition temperature was 1460 K. The higher temperature was expected since, for a lower oxygen level, a higher temperature will be needed to cause particle ignition. Also, it was found that a distribution of ignition temperature exists at each experimental condition. This is believed to be a result of the particle-to-particle variations in reactivity and size among the coal sample.

The measured ignition temperatures were analyzed using the Distributed Activation Energy Model of Ignition, and the ignition rate constant was determined to have an average value of 73 kJ/mol with a standard deviation of 3.7 kJ/mol. It is imperative to collect an extensive set of ignition data in order to establish meaningful statistics for the extraction of ignition rate constants.

Impact on Infrastructure and Human Resources

This project has provided North Carolina A&T State University with enormous infrastructure benefits, including over $60,000 worth of major equipment. Items gained as a direct result of this project's support includes a Nd:YAG laser system and associated optics, optical benches and tables, various electronics, the wind tunnel used in this study, and a computer for data acquisition and analysis.

Indirectly, this project attracted the support of the Department of Mechanical Engineering in securing non-federal equipment funding. A digital oscilloscope, a digital pulse generator, and a PC-based data-acquisition system – items purchased for over $19,000 – were acquired as a result.

In terms of human resources, this project supported three graduate students with salary and tuition, and six undergraduate students with salary during its three-year span. The first graduate student received his MS degree in the second year of this project [6], and another graduate student will complete his degree requirements during the 1998-99 academic year.

Suggestions for Future Work

This project has demonstrated that particle temperature can be measured in our novel, laser-based ignition experiment, and that the data can be interpreted using a unique model of coal ignition. The model more realistically represents the ignition reactivity of the coals within a sample, and permits the extraction of meaningful ignition rate constants from the measured temperatures. The project period, being dominated by experiment development, did not permit enough coal types to be examined, nor did it permit more careful optimization of the pyrometry system. Thus, the major recommendations for future work are to:

1. refine the pyrometry system by improving the signal-to-noise ratio (e.g., by improving light collection and transmission efficiency) to permit the use of more widely separated filter wavelengths in order to improve temperature-measurement accuracy;
2. make additional measurements of ignition rate constants for a variety of coals and a range of particle sizes and oxygen concentrations in order to establish a large database of ignition temperatures for statistical analysis using the DAEMI;
3. develop a means to compare the rate constants from this experiment with previously reported rate constants, which relied on different experimental techniques and methods of data analyses.

Our final recommendation is for the extension of this project's products – the ignition rate constants and the Distributed Activation Energy Model of Ignition – into practical applications. For example, these products may be incorporated into a model of the ignition of clouds of coal particles, which would be of obvious benefit in the design of low-NOx burners and the prevention of coal dust in mine shafts. Incorporation of the concepts and methods developed from this project would more realistically model the fuel characteristics with regard to reactivity distribution,

and could possibly lead to new insights on flame propagation otherwise unobtainable using more simplistic averaging to describe reactivity.

References

1 Essenhigh, R.H., Mahendra, K.M., and Shaw, D.W. *Combust. Flame*, 77:3-30 (1989).

2 Hurt, R.H. *Energy Fuels*, 7:721-733 (1993).

3 Chen, J.C. "Distributed Activation Energy Model of Heterogeneous Coal Ignition," *Combust. Flame*, 107, 291 (1996).

4 Chen, J.C., Taniguchi, M., Narato, K., and Ito, K. *Combust. Flame* 97:107-117 (1994).

5 Zhang, D., Wall, T.F., Harris, D.J., Smith, I.W., Chen, J., and Stanmore, B.R. *Fuel*, 71:1239-1246 (1992).

6 Musti, Subrahmanyam S. *Ignitability of Various Coals as Measured by Laser Ignition*, MS thesis, Department of Chemical Engineering, North Carolina A&T State University (1996).

Appendices

A. Reprint of published paper: "Distributed Activation Energy Model of Heterogeneous

(NOTE: This document available only in the hardcopy version of this report.)

Distributed Activation Energy Model of Heterogeneous Coal Ignition

John C. Chen
Department of Mechanical Engineering, North Carolina A&T State University, Greensboro, NC 27411

We present a model that simulates the conventional tube-furnace experiment used for ignition studies. The Distributed Activation Energy Model of Ignition accounts for particle-to-particle variations in reactivity by having a single preexponential factor and a Gaussian distribution of activation energies among the particles. The results show that the model captures the key experimental observations, namely, the linear increase in ignition frequency with increasing gas temperature and the variation of the slope of the ignition frequency with oxygen concentration. The article also shows that adjustments to the model parameters permit a good fit with experimental data. *Copyright © 1996 by The Combustion Institute*

NOMENCLATURE

A_0	preexponential factor in Arrhenius rate constant of ignition (kg m^{-2} s^{-1})
d	diameter (m)
E	activation energy of ignition (kJ mol^{-1})
E_0	mean of Gaussian distribution (kJ mol^{-1})
h	convective heat transfer coefficient (W m^{-2} K)
H_c	heat of reaction (J kg^{-1})
k	thermal conductivity (W m^{-1} K)
n	reaction order of ignition with respect to oxygen
Q	heat generated or heat loss (W)
R	universal gas constant (8.314 × 10^{-3} kJ mol^{-1} K^{-1})
S	external surface area of particle (m^2)
T	temperature (K)
y	molar ratio of CO to CO_2

Greek Symbols

χ_{O_2}	oxygen mole fraction at particle surface
ε	emissitivity of coal
σ_b	Stefan–Boltzmann constant (5.67 × 10^{-8} W m^{-2} K^{-4})
σ	standard deviation of Gaussian distribution (kJ mol^{-1})

Subscripts

conv	convection
g	gas
p	particle
rad	radiation

INTRODUCTION

Numerous experiments have been conducted over the past three decades to study the ignition of pulverized coals under conditions relevant to utility boilers. The conventional experiment is based on one developed by Cassel and Liebman [1], and consists of a tube furnace containing a heated mixture of O_2 and inert gas. The temperature of the furnace, and hence the gas, is the independent variable in this arrangement. The experiment is conducted by dropping a small batch of presized coal particles into the hot gas and visually observing for a flash of light, which signals ignition. In such an experiment the particle concentration is typically low enough that each particle can be considered to behave independently of all others. The furnace temperature is then decreased and the experiment is repeated to determine the *minimum gas temperature* (or the *critical gas temperature*) at which ignition occurs. This condition is termed *critical ignition*. Finally, the particle size or the O_2 concentration is changed and, again, the critical ignition condition is found for the new operating condition.

THEORY OF HETEROGENEOUS IGNITION

Essenhigh et al. [2] describe in detail the theory of heterogeneous ignition, that is, ignition that occurs at the solid–gas interface. For a coal particle exposed to an oxidizing environment, ignition is determined by the balance

COMBUSTION AND FLAME 107:291–298 (1996)
Copyright © 1996 by The Combustion Institute
Published by Elsevier Science Inc.

0010-2180/96/$15.00
PII S0010-2180(96)00056-9

between heat generation at and heat loss from the particle surface. The heat loss from the surface of a particle at temperature T_p is the sum of the losses caused by convection and radiation:

$$Q_{\text{loss}} = Q_{\text{loss,conv}} + Q_{\text{loss,rad}} = hS(T_p - T_g) + \varepsilon\sigma_b S\left(T_p^4 - T_g^4\right). \quad (1)$$

Equation 1 assumes that the surroundings involved in radiation exchange are in thermal equilibrium with the gas.

The radiative loss term is relatively unimportant until the particle temperature exceeds ~ 1500 K. For the convective-loss term, we assume that the Nusselt number equals 2, as is appropriate for very small particles, which leads to $h = 2k_g/d_p$. Thus, Eq. 1 can be rewritten, on a per-external-surface-area basis, as:

$$\frac{Q_{\text{loss}}}{S} = \frac{2k_g}{d_p}(T_p - T_g) + \varepsilon\sigma_b\left(T_p^4 - T_g^4\right). \quad (2)$$

The gas thermal conductivity, k_g, in the boundary layer around a heated particle is given by a linear fit to the conductivity of air over the temperature range of 300–2000 K:

$$k_g = 7.0 \times 10^{-5}\left[\frac{T_p + T_g}{2}\right]\frac{\text{W}}{\text{m K}}. \quad (3)$$

Equation 3 represents an approximation for the conductivity evaluated at the mean of the free-stream and particle-surface temperatures, and it is noted that the variation of conductivity with temperature may be represented by higher order representations.

The heat generated by a spherical carbon particle undergoing oxidation on its external surface is given by the kinetic expression:

$$\frac{Q_{\text{gen}}}{S} = H_c\, \chi_{O_2}^n A_0 \exp\left[\frac{-E}{RT_p}\right]. \quad (4)$$

Diffusion effects are neglected because at the relatively low particle temperatures of pulverized-coal ignition, the oxidation reaction is kinetically controlled.

At the critical ignition condition, the following two conditions are satisfied [2]:

$$Q_{\text{gen}} = Q_{\text{loss}}, \quad (5)$$

$$\frac{dQ_{\text{gen}}}{dT_p} = \frac{dQ_{\text{loss}}}{dT_p}. \quad (6)$$

It is presumed for the purpose of this study that certain of the variables in Eqs. 2 and 4 are known a priori (H_c, A_0, n, d_p, and ε), or are fixed by the experimental conditions (T_g and χ_{O_2}). The values of these variables used for the base case (described below) are shown in Table 1. The remaining unknowns, T_p and E, can then be determined by the simultaneous solution of Eqs. 5 and 6; the relation of these two parameters to T_g for the base case is shown in Fig. 1. T_p determined in this manner represents the critical ignition temperature, whereas E can be interpreted as the critical (or maximum) activation energy that a particle may have and still ignite under the given conditions. A detailed expansion of Eqs. 5 and 6 is given in the Appendix.

MODEL FORMULATION

Figure 2 shows typical data [3] obtained from an ignition experiment conducted by varying the gas temperature while holding all other

TABLE I

Values of Parameters in the Base Case of the Model

Variable	Value	Units	Remarks
A_0	500	kg m^{-2} s^{-1}	arbitrarily chosen to illustrate model
d_p	100	μm	arbitrarily chosen to illustrate model
E_0	120	kJ mol^{-1}	arbitrarily chosen to illustrate model
H_c	9210	kJ kg^{-1}	for the reaction C + 1/2 O_2 → CO
n	1.0	—	arbitrarily chosen to illustrate model
σ	16.0	kJ mol^{-1}	arbitrarily chosen to illustrate model
ε	0.8	—	arbitrarily chosen to illustrate model

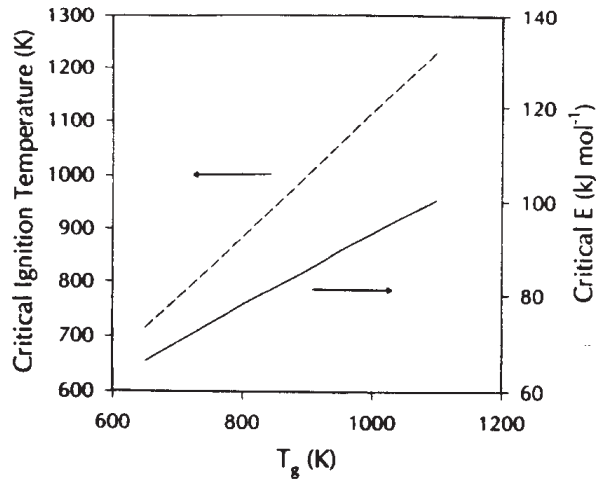

Fig. 1. Relation of critical ignition temperature (dashed line) and critical activation energy (solid line) to gas temperature, T_g, for base case listed in Table 1.

parameters constant. The data shown was obtained by conducting the experiment as described earlier except that, at each temperature, 10 to 20 tests for ignition were repeated to obtain a frequency or probability of ignition. Fig. 2 shows that ignition frequency increases approximately linearly with gas temperature, and this is inconsistent with the heterogeneous ignition theory previously described. If all particles of a coal sample used in an experiment have the same reactivity, that is, they are described by a common Arrhenius rate constant as in Eq. 4, then the data would show an ignition frequency of 0% until the critical gas temperature, corresponding to that at the critical ignition condition, is reached. At any gas temperature above this, the ignition frequency would be 100%. Note that the observed ignition frequency trend is not an artifact of the experiment; this same behavior is reported from a variety of ignition experiments [4, 5, 6] including thermogravimetric analyzers and laser-based studies.

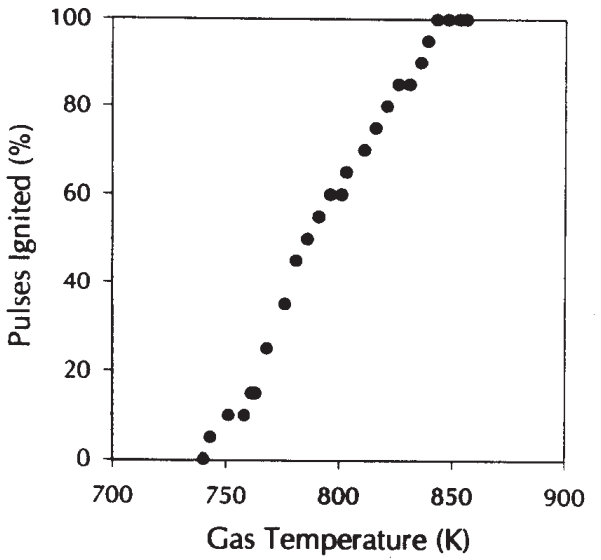

Fig. 2. Typical data from a conventional ignition experiment showing the relation between ignition frequency (or probability) and gas temperature for a bituminous coal. Data extracted from Ref. 3.

One of the reason why ignition frequency should increase gradually with increasing gas temperature is somewhat obvious: Within any sample of coal, there exists a *distribution of reactivity* among the particles. Thus, in the conventional ignition experiment, in which a batch of perhaps a few hundred particles of a sample is dropped into the furnace, there is an increasing probability (or frequency) that at least one particle has a reactivity that meets or exceeds the critical ignition condition set forth in Eqs. 5 and 6 as the gas temperature is increased. Of course, there exist other variations among the particles within a sample, such as particle size and specific heat. Variation in size alone could account for the observed increase in ignition frequency with gas temperature. It cannot account for another experimental observation, however, namely the variation in the slope of the ignition frequency with oxygen concentration. (This behavior is described in a later section.) A distribution in specific heat would only affect the rate at which a particle attains its equilibrium temperature, but would not change this value or the reactivity. Perhaps other variations could cause the observed behavior of ignition frequency. It is our premise that the distribution in reactivity dominates all other variations, however, and therefore accounts for the observed behavior.

The Distributed Activation Energy Model of Ignition (DAEMI) models the conventional ignition experiment by allowing for the particles within the coal sample to have a distribution of reactivity. We prescribe that all the particles have the same properties, including the preexponential factor in the Arrhenius rate constant describing their ignition reactivity, and that their activation energy is distributed according

to the Gaussian (or normal) distribution:

$$f(E) = \frac{1}{(2\pi\sigma^2)^{0.5}} \exp\left[\frac{-(E - E_0)^2}{2\sigma^2}\right] \quad (7)$$

where E_0 is the mean and σ is the standard deviation of the distribution. The expression

$$\int_E^{E+\Delta E} f(E)\, dE \quad (8)$$

describes the frequency or probability that particles within a sample have an activation energy in the range E to $E + \Delta E$. Accordingly, the distribution satisfies the condition that $\int_{-\infty}^{\infty} f(E)\, dE = 1$.

The DAEMI divides a prescribed distribution into discrete energy intervals of $\Delta E = 3$ kJ mol^{-1}, and considers only the energy range of $E_0 - 3\sigma$ to $E_0 + 3\sigma$, rather than $-\infty$ to $+\infty$. The latter simplification still covers 99.73% of the distribution. The model then calculates the frequency of being in each of these intervals by numerically integrating Eq. 8 for each of the intervals.

An ignition experiment is modeled by assuming that 10^5 particles are in the initial sample, and that they are distributed among the various ΔE intervals according to the calculated frequency for each interval. Each simulation of an experimental run under a given set of conditions is conducted on a batch of 100 randomly selected particles from the sample, keeping in mind that no particle can be selected more than once. Whether or not ignition occurs for a run is determined by the particle in the batch of 100 with the lowest activation energy. If this particle's reactivity equals or exceeds that determined by the critical ignition condition (that is, its activation energy is less than or equal to the critical energy determined by solution of Eqs. 5 and 6), the batch is defined as ignited. This is consistent with our observation [6] that single-particle ignition is discernible to the eye, and certainly to a photon detector. This procedure is repeated 20 times at each condition, just as in actual experiments, to determine an ignition frequency at this condition. Finally, the gas temperature is varied several times and, each time, 20 runs are conducted.

RESULTS AND DISCUSSION

Figure 3 shows model results of ignition frequency versus gas temperature for one hypothetical sample for which $E_0 = 120$ kJ mol^{-1}, $\sigma = 16$ kJ mol^{-1}, and $A_0 = 500$ kg m^{-2} s^{-1}. The other parameters of this base case calculation are listed in Table 1. It is obvious that the DAEMI exhibits the experimental characteristic of increasing ignition frequency with increasing gas temperature. As stated earlier, this is expected as an increase in gas temperature leads to an increase in the maximum activation energy that a particle can have and still be ignitable (see Fig. 1), and therefore to an increased probability of having at least one particle within each batch of a simulated run that is reactive enough to ignite.

Figures 4 and 5 display the effects of varying E_0 and σ, respectively, on the DAEMI. An increase in E_0, which shifts the Gaussian distribution to higher energies (Fig. 4a), has the effect of shifting the ignition-frequency data to higher gas temperatures (Fig. 4b). This is the expected behavior as a representative batch from the higher E_0 sample contains, on average, particles with higher activation energies, which require a higher temperature to induce ignition. Note that E_0 has only a slight effect on the slope of the data in Fig. 4b.

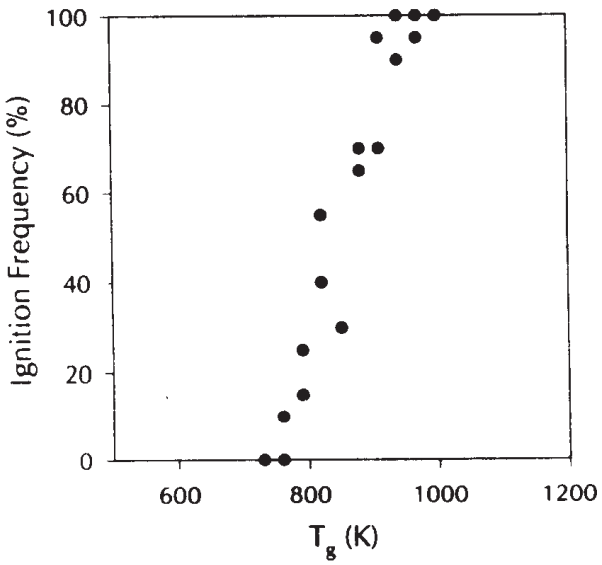

Fig. 3. Results from Distributed Activation Energy Model of Ignition (DAEMI) for base case (Table 1).

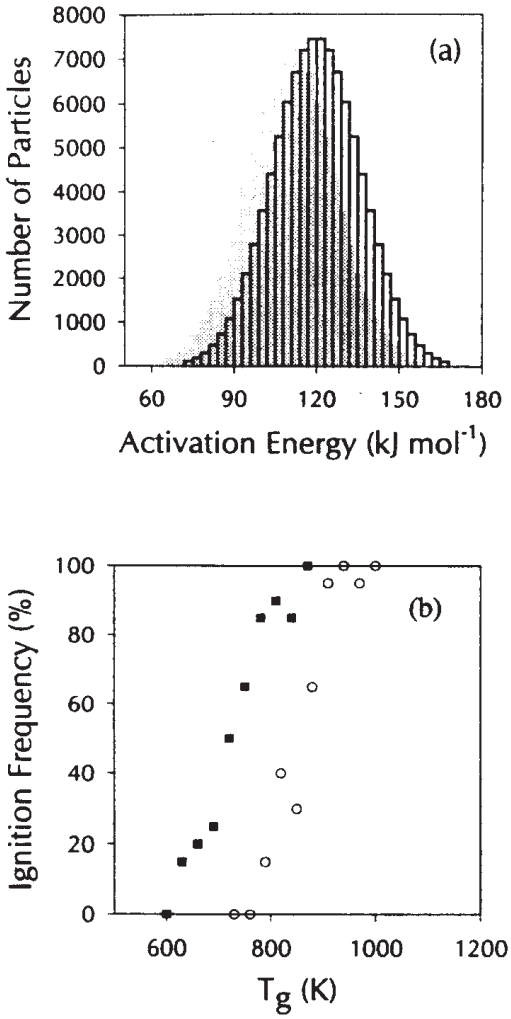

Fig. 4. DAEMI results showing the effect of E_0 on ignition frequency. (a) Solid-colored distribution corresponds to E_0 = 110 kJ mol^{-1}, and the distribution shown in outline corresponds to E_0 = 120 kJ mol^{-1}; all other parameters are as listed in Table 1. (b) Ignition frequency data for E_0 = 110 kJ mol^{-1} (■) and E_0 = 120 kJ mol^{-1} (○).

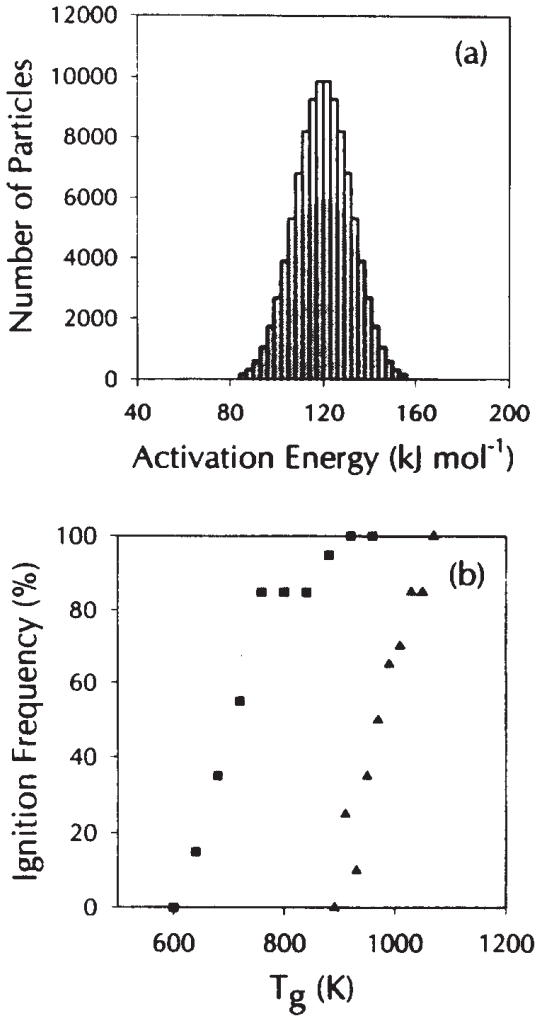

Fig. 5. DAEMI results showing the effect of σ on ignition frequency. (a) Solid-colored distribution corresponds to σ = 20 kJ mol^{-1}, and the distribution shown in outline corresponds to σ = 12 kJ mol^{-1}; all other parameters are as listed in Table 1. (b) Ignition frequency data for σ = 20 kJ mol^{-1} (■) and σ = 12 kJ mol^{-1} (▲).

Figure 5 shows that an increase in the standard deviation (σ)—the spread of the Gaussian distribution (Fig. 5a)—has two effects: a shift of the ignition frequency to lower temperatures and a slower rise of ignition frequency with gas temperature (Fig. 5b). These findings are somewhat unexpected because the average activation energy (E_0) is the same for both samples, and they result from the use of a small batch (100 particles) in each run. The shift to lower temperatures is caused by the fact that, statistically, the most reactive particle in the larger σ batch will have a lower activation energy than the most reactive particle from the smaller σ batch because of its wider spread in distribution. Thus, the higher reactivity allows for ignition to occur at lower temperatures. The wider spread and small batch also cause the slower approach to 100% ignition frequency because the probability of having a batch containing only relatively higher energy particles is increased, which requires higher gas temperatures until all runs result in ignition. Clearly, by adjusting the two parameters of the Gaussian distribution (Eq. 7), E_0 and σ, the DAEMI can be fitted to ignition data, such as those in Fig. 2, provided that accurate val-

ues for the parameters shown in Table 1 are available.

The DAEMI in its present form fails to capture a second experimental characteristic, namely, the change in slope of the ignition frequency data with oxygen concentration, as shown in Fig. 6. The lines shown are linear regressions of experimental data from Ref. 3. (The data points are explained below.) In fact, the DAEMI shows a very weak dependence on oxygen concentration (not shown), so the question remains as to what parameter has not been or is incorrectly accounted for. The obvious candidate is the reaction order, n, which must vary with χ_{O_2} in order to cause the observation. We can think of no fundamental basis for this behavior, however.

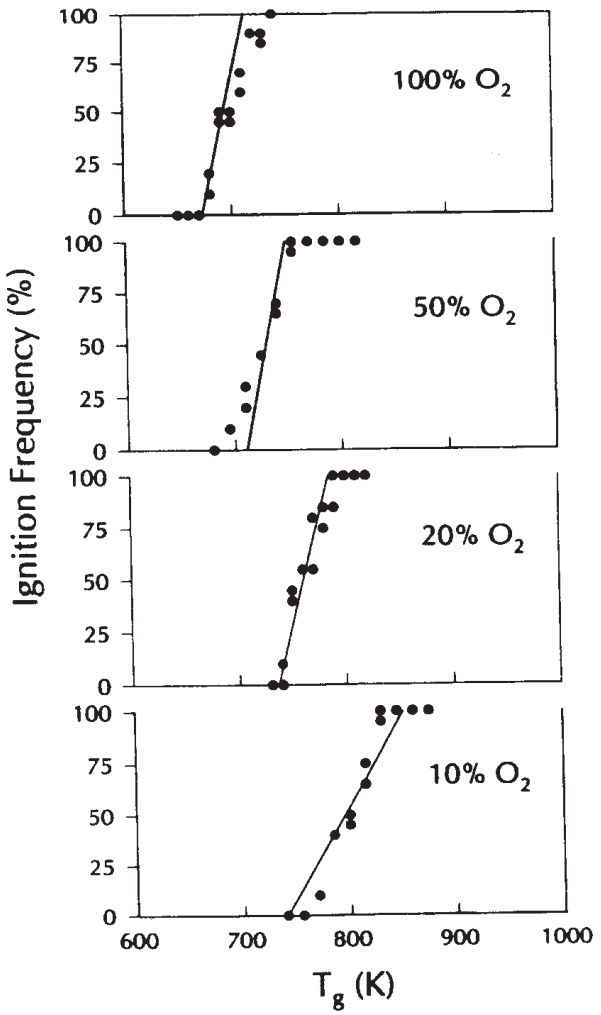

Fig. 6. Linear regressions of experimental data from Ref. 3 (shown as solid lines), showing the effect of free-stream oxygen concentration on ignition of a high-volatile bituminous coal of diameter 75–90 μm. The data points represent results from the DAEMI, including the modification to account for the production of both CO and CO_2 and adjustments to the base case values for E_0, σ, and n, as described in the text.

A second, less obvious parameter is the heat of reaction, H_c, of ignition. So far in the presentation of the DAEMI, it has been assumed that the product of coal ignition is CO, as shown by the value for H_c in Table 1. It is well known that the product of carbon oxidation is both CO and CO_2, however, with the relative amounts dependent on both temperature and oxygen partial pressure [7, 8]. The significance of this is that their heats of reaction are vastly different:

$$\begin{aligned} C + \frac{1}{2}O_2 \rightarrow CO;\ H'_{C,CO} &= 9{,}210\frac{kJ}{kg\ C} \\ C + O_2 \rightarrow CO_2;\ H'_{C,CO_2} &= 32{,}790\frac{kJ}{kg\ C} \end{aligned} \tag{9}$$

Thus, the value of H_c in Eq. 4 is dependent on the relative amounts of CO and CO_2 formed during ignition, and is given by the expression:

$$H_C = \frac{y}{y+1}H'_{C,CO} + \frac{1}{y+1}H'_{C,CO_2}, \tag{10}$$

where y = mol CO/mol CO_2. We have assumed here that energy released by any CO that oxidizes as it diffuses away from the particle surface does not affect the ignition.

This modification to the DAEMI should now show the experimental trend. Measurements [7, 8] show that at higher particle temperature (which results from higher T_g), the molar ratio CO/CO_2 increases and consequently H_c, the amount of heat released during ignition, decreases. Therefore, the result of a set of runs conducted at a decreased oxygen level not only shifts the ignition frequency data to a higher T_g (a direct result of the decreased χ_{O_2}) but also reduces the slope of the rise (an indirect result because of the decreased H_c).

Direct measurements of the CO/CO_2 ratio have been made by Du et al. [7] in a thermogravimetric analyzer (TGA) using soot as the carbon material. Measurements were made over the temperature range of 667–873 K and

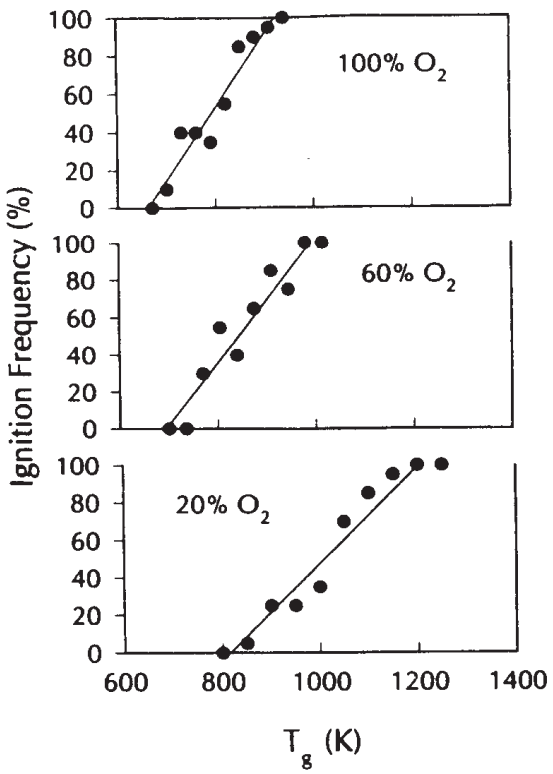

Fig. 7. DAEMI results, including the modification to account for the production of both CO and CO_2, showing the effect of oxygen concentration on ignition frequency. The solid lines indicate linear regressions of the data points.

oxygen partial pressures from 0.1 to 1 atm. The results at an oxygen partial pressure of 0.21 atm are correlated by the expression:

$$\frac{\text{mol CO}}{\text{mol CO}_2} = 59.95 \exp\left[\frac{-3214}{T_p(\text{K})}\right] \tag{11}$$

This correlation is incorporated into the DAEMI and the model results are shown in Fig. 7. Notice that the model now clearly possesses the desired characteristic. Furthermore, it captures *both* the decrease in the slope of the ignition frequency with decreasing oxygen concentration, and the slow rate of the slope's decrease until low oxygen concentrations, showing the nonlinear behavior with χ_{O_2} displayed in experimental data (Fig. 6).

By adjusting the mean, the standard deviation and the reaction order, n, of the base case, this current version of DAEMI can be fit to the experimental data shown in Fig. 6. (The particle diameter has also been changed to 83.0 μm to match the mean of the sample used in Ref. 3.) The model results using $E_0 = 84.0$ kJ mol^{-1}, $\sigma = 4.0$ kJ mol^{-1}, and $n = 0.4$, are plotted as data points in Fig. 6 over the regression lines and show that a satisfactory fit is achieved with minimal effort in parameter adjustment, despite the uncertainties in the values of other parameters. (Because of the small value of σ used, the energy intervals into which the distribution is divided was decreased from 3 kJ mol^{-1} to 1 kJ mol^{-1} to obtain these results.) It should be noted that the ignition parameters reported above represent merely a rough fit to the experimental data; it is certainly possible that another set of parameters can also fit the data satisfactorily, especially if a different value for A_0 were chosen. This extra effort may be worthwhile as certain parameters have strong theoretical justification (the reaction order, n, for example) for being within a particular range. We have begun work to examine this issue in more detail.

Although we have assumed in this study that pulverized-coal ignition occurs heterogeneously without influence from any volatile matter that may be present, and even though the results closely fit the experimental data, it cannot be said that the DAEMI confirms that ignition is purely a heterogeneous process. Very few models of homogeneous ignition have been presented, and none have been tested against the available experimental data because of the inherent difficulty and uncertainty in modeling devolatilization and the combined solid- and gas-phase reactions.

CONCLUSIONS

The DAEMI has been formulated to model conventional coal-ignition experiments. It accounts for particle-to-particle variations in reactivity within a sample by allowing for a distribution in activation energies among the particles and a single preexponential factor.

The model captures the main characteristics of actual experiments: the gradual increase in ignition frequency with increasing gas temperature and the variation of the slope of the ignition frequency with O_2 concentration. Finally, it has been shown that adjustments to the model parameters can be used to fit experi-

mental data and extract reaction rate constants.

The support of the U.S. Department of Energy (Grant DE-FG22-94MT94013) for this project is gratefully acknowledged.

REFERENCES

1. Cassel, H. M., and Liebman, I. *Combust. Flame* 3:467–475 (1959).
2. Essenhigh, R. H., Mahendra, K. M., and Shaw, D. W., *Combust. Flame* 77:3–30 (1989).
3. Zhang, D., Wall, T. F., Harris, D. J., Smith, I. W., Chen, J., and Stanmore, B. R., *Fuel* 7:1239–1246 (1992).
4. Tomeczek, J., and Wojcik, J., *Twenty-Third Symposium (International) on Combustion*, The Combustion Institute, Pittsburgh, 1990, pp. 1163–1167.
5. Boukara, R., Gadiou, R., Gilot, P., Delfosse, L., and Prado, G., *Twenty-Fourth Symposium (International) on Combustion*, The Combustion Institute, Pittsburgh, 1993, pp. 1127–1133.
6. Chen, J., Taniguchi, M., Narato, K., and Ito, K., *Combust. Flame* 97:107–117 (1994).
7. Du, Z., Sarofim, A. F., and Longwell, J. P., *Energy and Fuels* 5:214–221 (1991).
8. Mitchell, R. E., Kee, R. J., Glarborg, P., and Coltrin, M. E., *Twenty-Third Symposium (International) on Combustion*, The Combustion Institute, Pittsburgh, 1990, pp. 1169–1176.

Received 30 July 1995; accepted 4 February 1996

APPENDIX

Expansion of Eqs. 5 and 6

In order to determine the critical ignition temperature of the particle, T_p, and critical activation energy, E, Eqs. 5 and 6 are solved simultaneously. Q_{gen} and Q_{loss} are given in Eqs. 2 and 4, and lead to the following derivatives with respect to temperature:

$$\frac{dQ_{gen}}{dT_p} = SH_c \chi_{O_2}^n A_0 \exp\left[\frac{-E}{RT_p}\right]\left(\frac{E}{RT_p^2}\right) \quad (12)$$

$$\frac{dQ_{loss}}{dT_p} = \frac{2k_g}{d_p}S + 4\varepsilon\sigma_b S T_p^3. \quad (13)$$

Note that the neglect of the T_p dependence in k_g introduces a small error in Eq. 13.

Following Eq. 6, we set Eq. 12 equal to Eq. 13 and solve for the quantity E/RT_p:

$$\frac{E}{RT_p} = \frac{\frac{2k_g}{d_p}T_p + 4\varepsilon\sigma_b T_p^4}{H_c \chi_{O_2}^n A_0 \exp\left[\frac{-E}{RT_p}\right]}. \quad (14)$$

The denominator is recognized to be Q_{gen}/S (Eq. 4), which by Eq. 5 is also Q_{loss}/S (Eq. 2). Thus Eq. 14 can be rewritten as:

$$\frac{E}{RT_p} = \frac{\frac{2k_g}{d_p}T_p + 4\varepsilon\sigma_b T_p^4}{\frac{2k_g}{d_p}(T_p - T_g) + \varepsilon\sigma_b\left(T_p^4 - T_g^4\right)}. \quad (15)$$

This relation for E/RT_p is substituted into the expression $Q_{gen} - Q_{loss} = 0$ to obtain a function, F, which is a function of T_p only:

$$\begin{aligned} F(T_p) &= Q_{gen} - Q_{loss} \\ &= H_c \chi_{O_2}^n A_0 \\ &\quad \times \exp\left[\frac{\frac{-2k_g}{d_p}T_p - 4\varepsilon\sigma_b T_p^4}{\frac{2k_g}{d_p}(T_p - T_g) + \varepsilon\sigma_b\left(T_p^4 - T_g^4\right)}\right] \\ &\quad - \frac{2k_g}{d_p}(T_p - T_g) - \varepsilon\sigma_b\left(T_p^4 - T_g^4\right) = 0. \end{aligned} \quad (16)$$

The reasonable root of $F(T_p)$ corresponds to the critical ignition temperature of the particle, and substitution of this value into Eq. 15 produces the critical activation energy at the critical ignition condition.

modified 9/19/94

VERTICAL WIND TUNNEL

- DRAWING NOT TO SCALE

DR. CHEN.

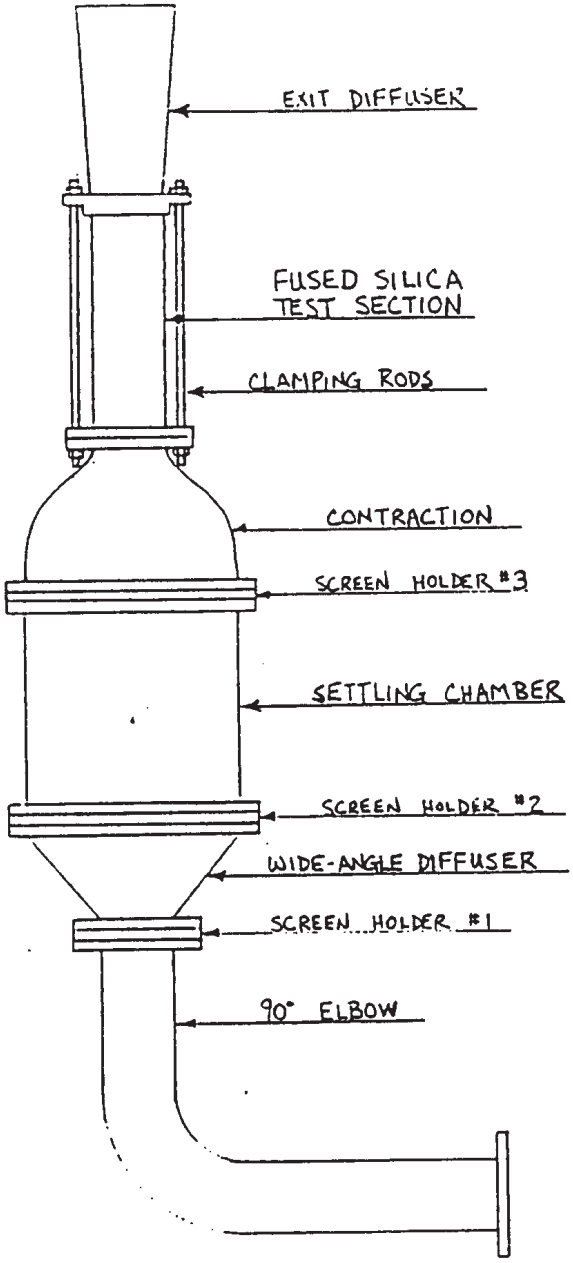

H4 - Z-1
John Chen
ジョン・チェン
GR2

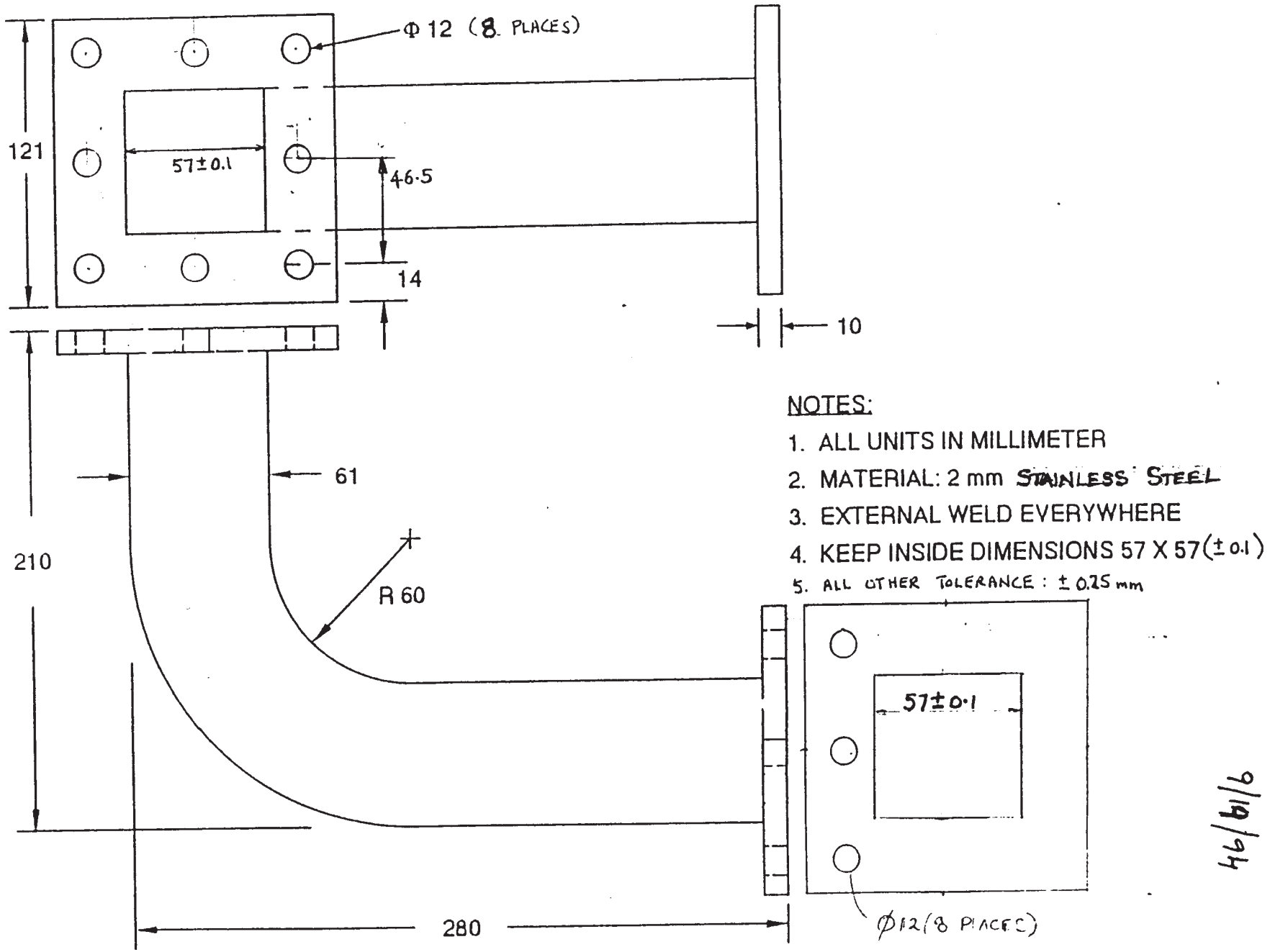

NOTES:

1. ALL UNITS IN MILLIMETER
2. MATERIAL: 2 mm STAINLESS STEEL
3. EXTERNAL WELD EVERYWHERE
4. KEEP INSIDE DIMENSIONS 57 X 57(±0.1)
5. ALL OTHER TOLERANCE : ± 0.25 mm

9/19/94

9/19/94

SCREEN HOLDER # 1 (50×50 round)

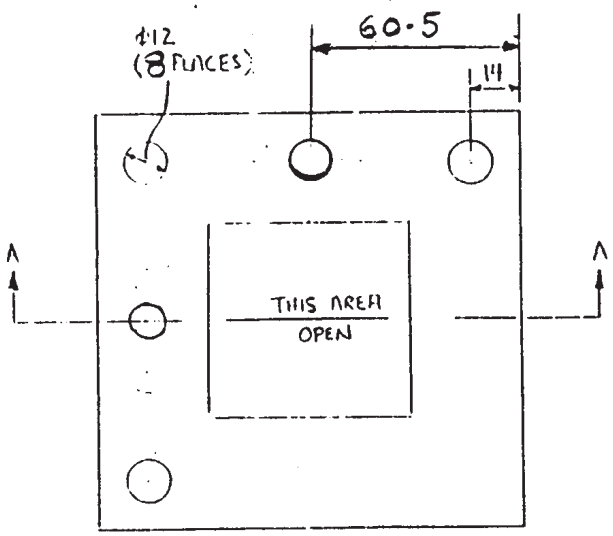

SECTION A-A

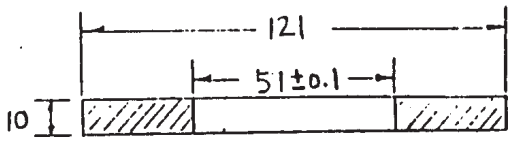

NOTES:

1) ALL UNITS IN MILLIMETER

3) MATERIAL : STAINLESS STEEL

4) ALL TOLERANCE : ±0.25mm, except as noted on DRAWING

11-2-3
John Chen
GR 2

9/19/94

WIDE-ANGLE DIFFUSER (50x50 TUNNEL)

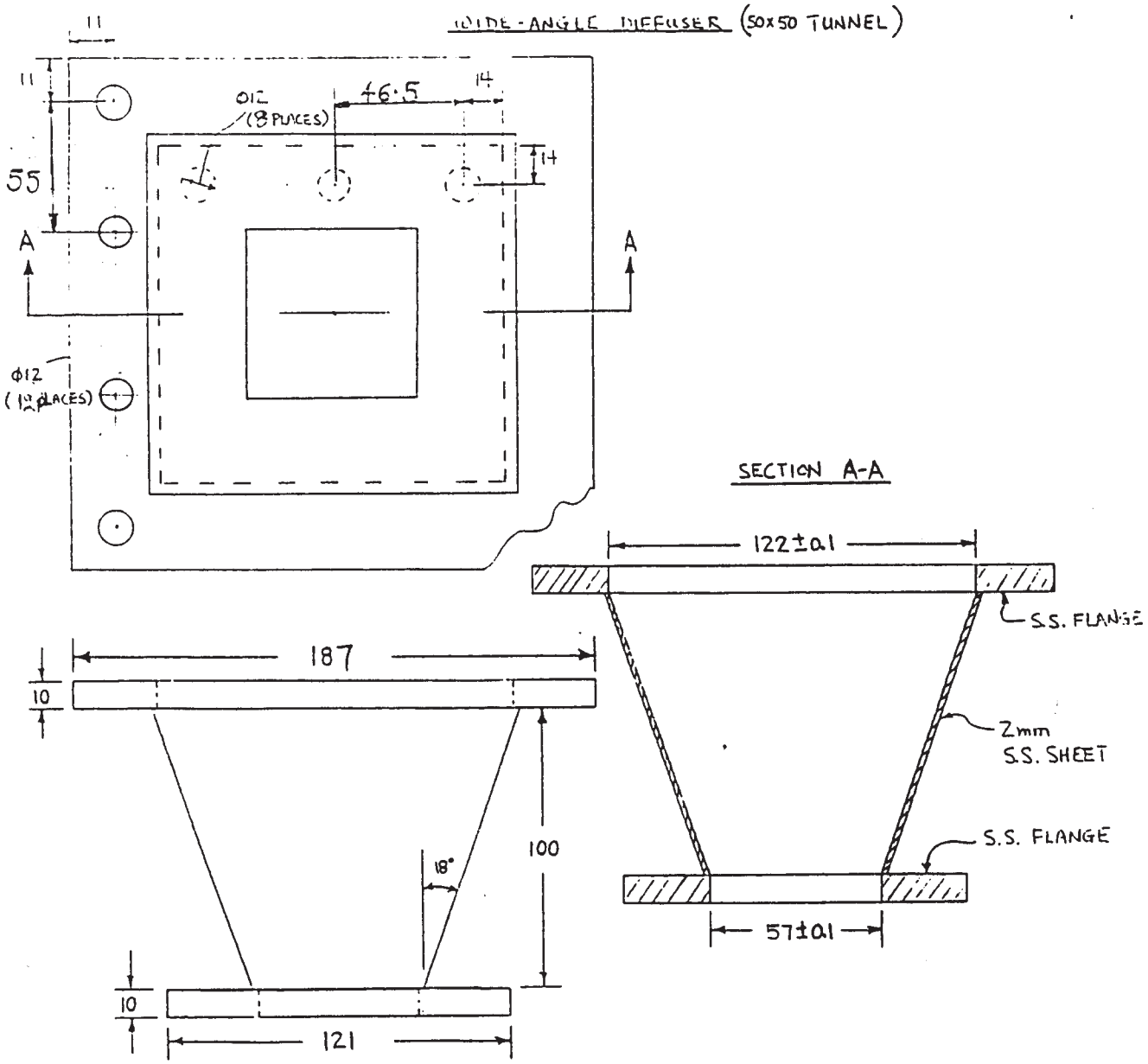

NOTES

1) ALL UNITS IN MILLIMETER

3) EXTERNAL WELDS ONLY

4) ALL TOLERANCE : ± 0.25 mm, EXCEPT WHERE NOTED ON DRAWING

H4-2-1
John Chen
GR2

9/19/94

SCREEN HOLDER #2 (50×50 TUNNEL)

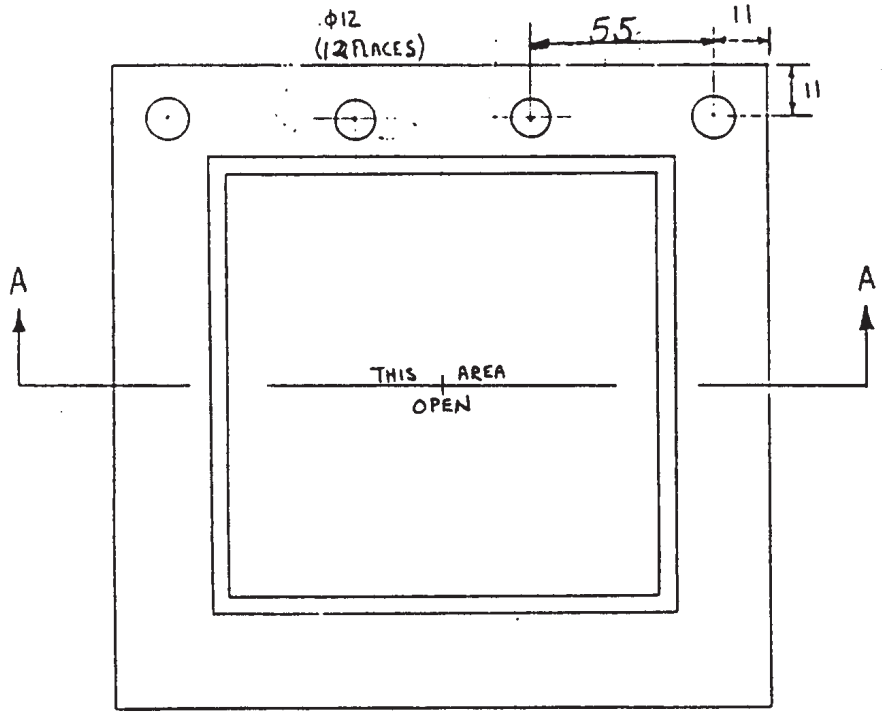

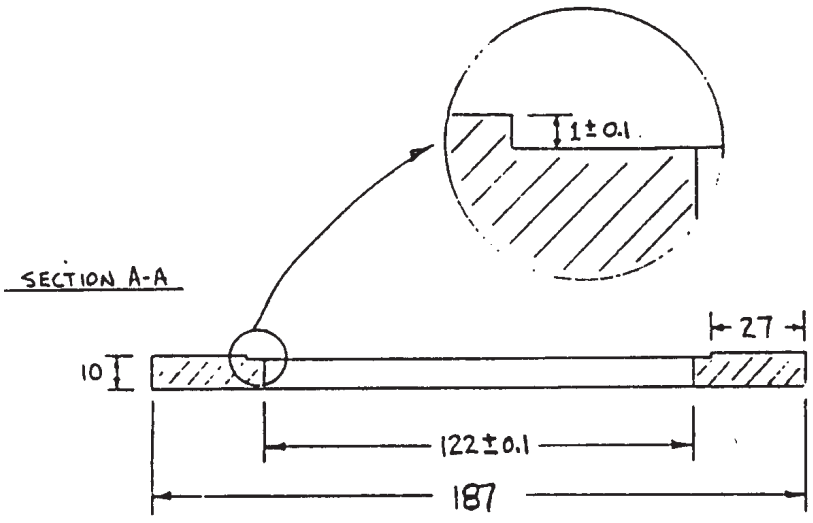

SECTION A-A

NOTES:

1) ALL DIMENSIONS IN MILLIMETER

3) MATERIAL: STAINLESS STEEL

4) ALL TOLERANCE: ±0.25mm EXCEPT WHERE NOTED ON DRAWING

H4·2·4
John Chen
GC2

1/1 · 2·5
John Chen
GR 2

9/19/94

SETTLING CHAMBER (50×50 TUNNEL)

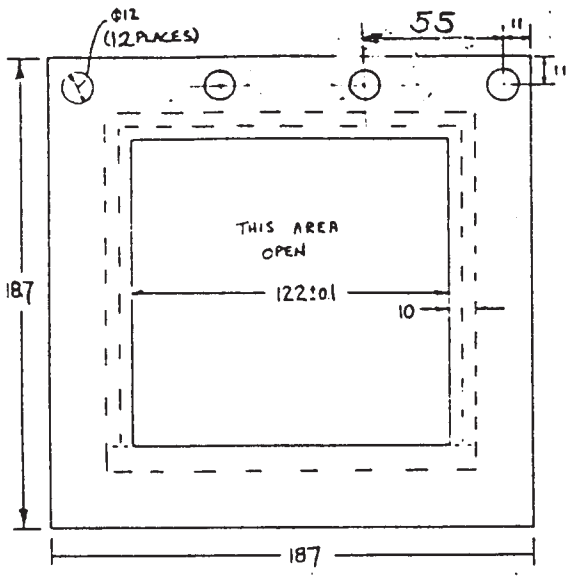

NOTES:
1) ALL DIMENSIONS IN MILLIMETER
3) MATERIAL: STAINLESS STEEL
4) EXTERNAL WELDS ONLY
5) ALL TOLERANCE: ± 0.15mm UNLESS OTHERWISE NOTED ON DRAWING

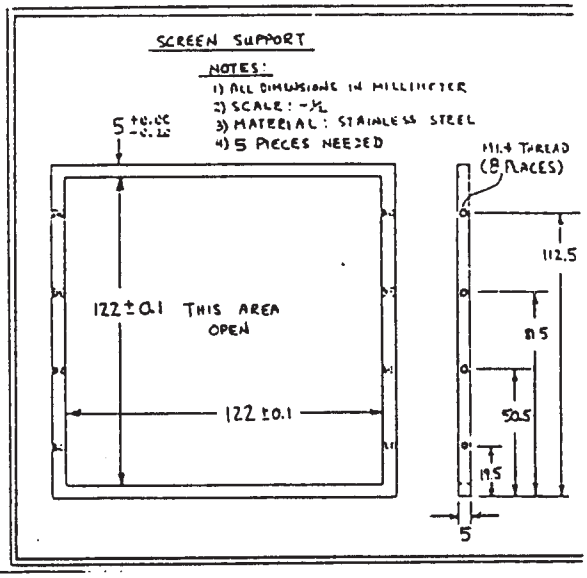

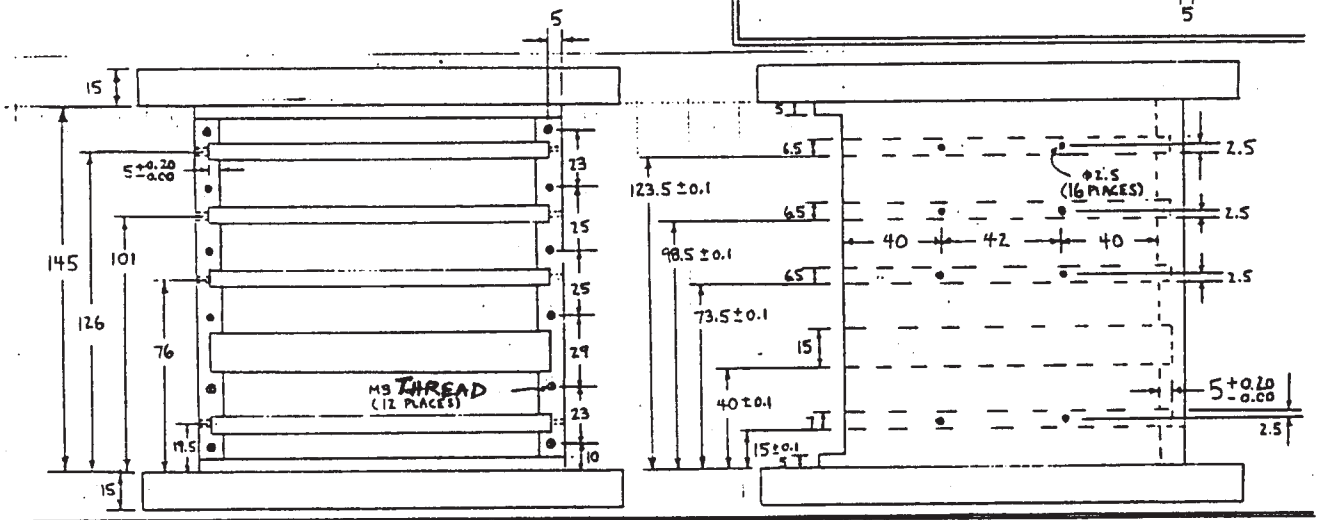

SETTING CHAMBER DOOR

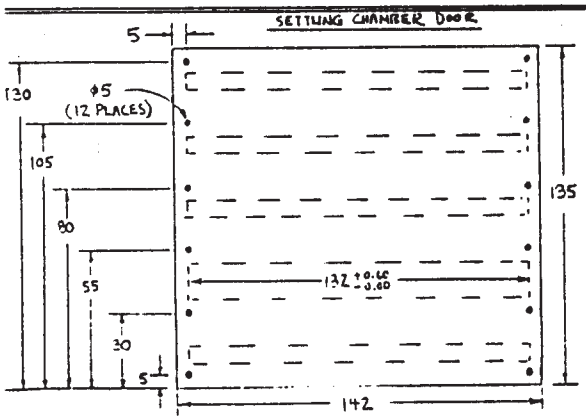

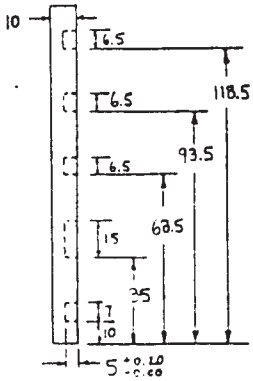

NOTES:
1) ALL DIMENSIONS IN MILLIMETER
2) NOT TO SCALE
3) MATERIAL: STAINLESS STEEL
4) ALL TOLERANCE: ± 0.1 mm, EXCEPT WHERE NOTED ON DRAWING

9/19/94.

SCREEN HOLDER #3 (50x50 TUNNEL)

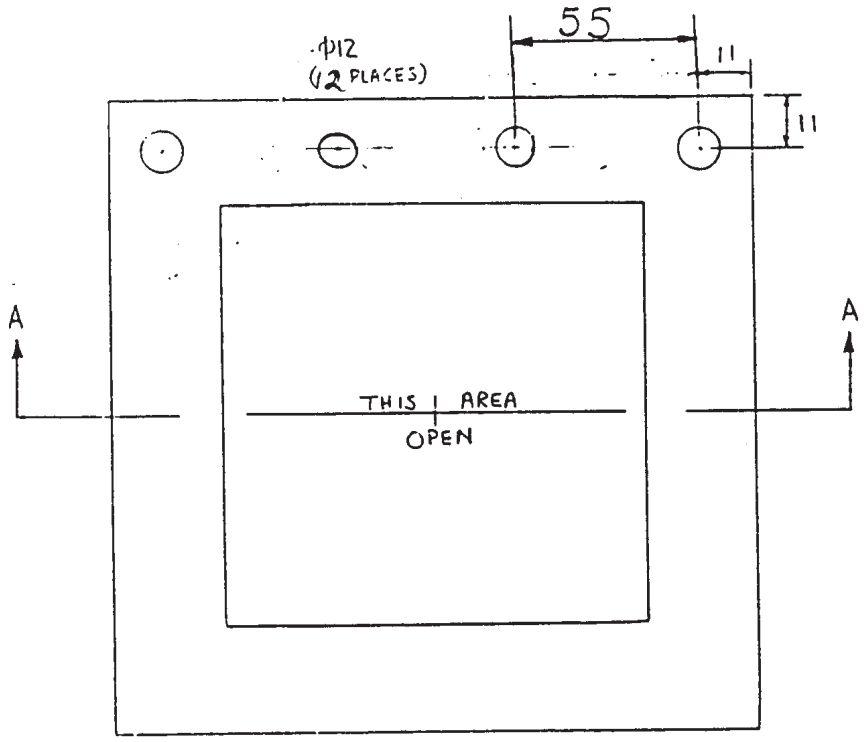

NOTES:
1) ALL DIMENSIONS IN MILLIMETER
3) MATERIAL : STAINLESS STEEL
4) ALL TOLERANCE : ±0.25 mm, EXCEPT AS NOTED ON DRAWING

SECTION A-A

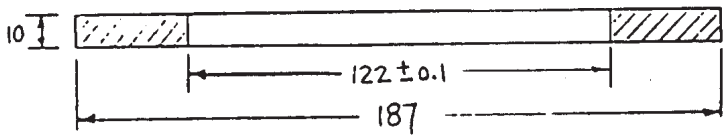

H4-2-4
John Chen
GR 2

9/19/94

CONTRACTION (50 x 50 TUNNEL)

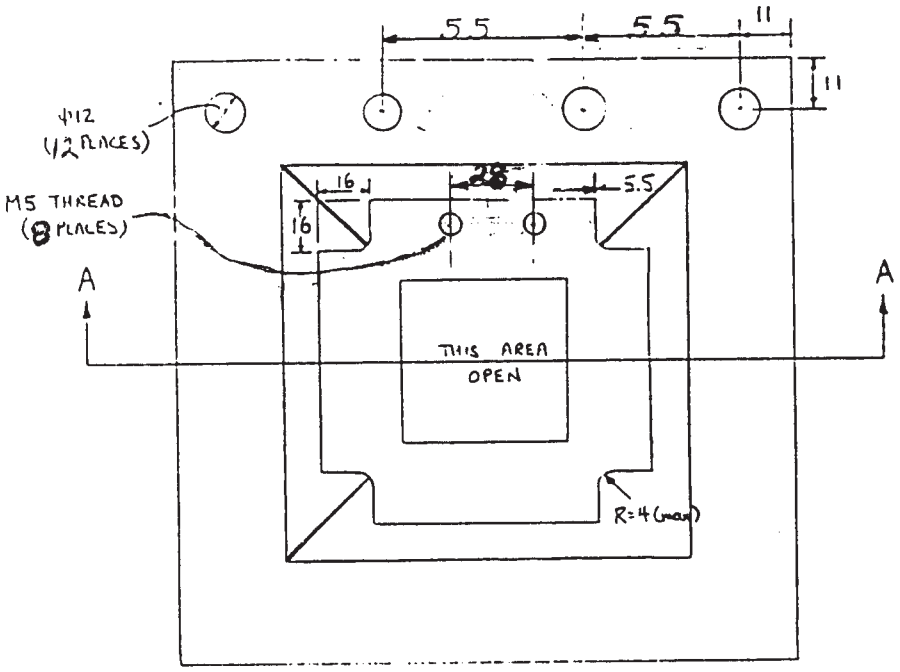

SECTION A-A

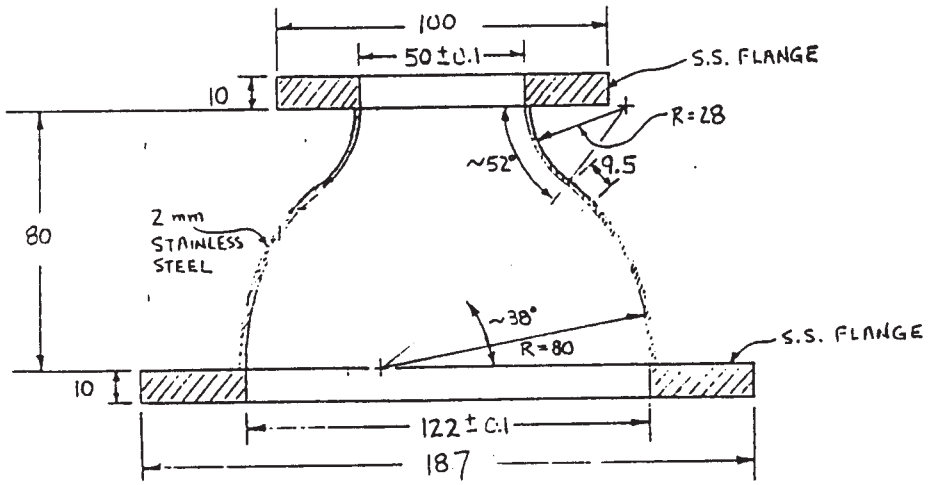

NOTES

1) ALL DIMENSIONS IN MILLIMETER

3) EXTERNAL WELDS ONLY

4) ALL TOLERANCE: ± 0.2 mm, EXCEPT [illegible] NOTED ON DRAWING

H4-Z-4
John Chen
GR2

9/19/94

FLANGE - TEST SECTION ENTRANCE (50 x 50 TUNNEL)

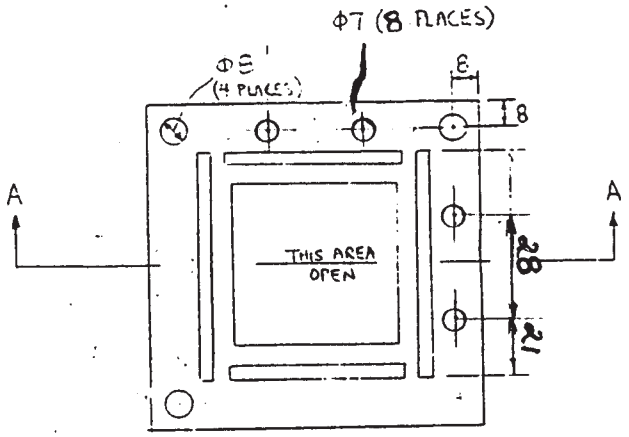

SECTION A-A

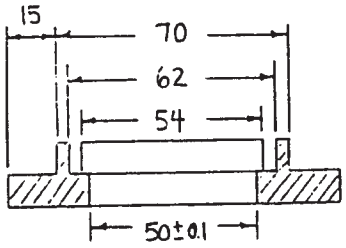

NOTES:

1) ALL UNITS IN MILLIMETER

3) MATERIAL STAINLESS STEEL

4) ALL TOLERANCE: ±0.25mm, EXCEPT WHERE NOTED ON DRAWING

H4-2-3
John Chen
Gr 2

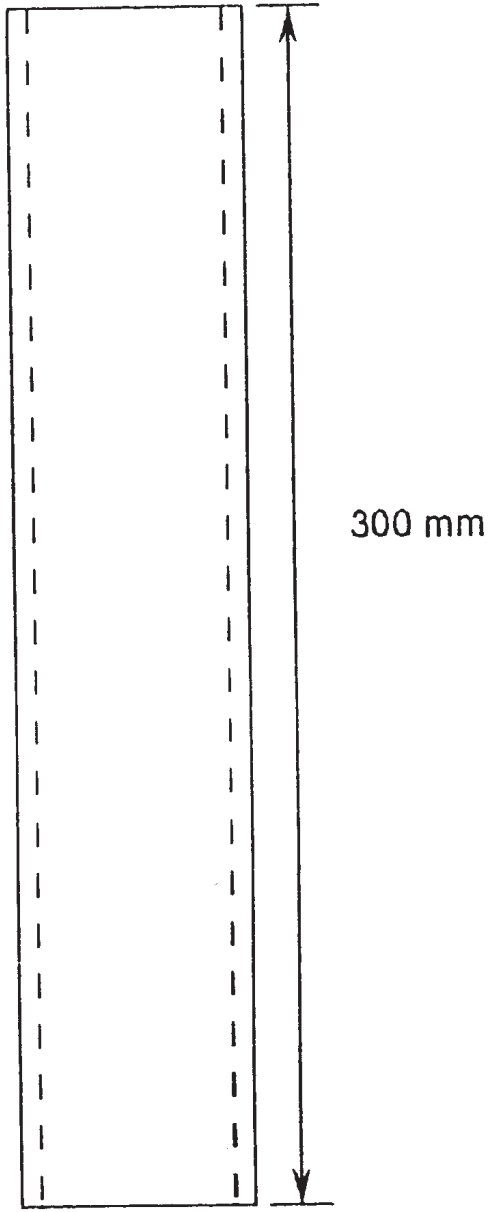

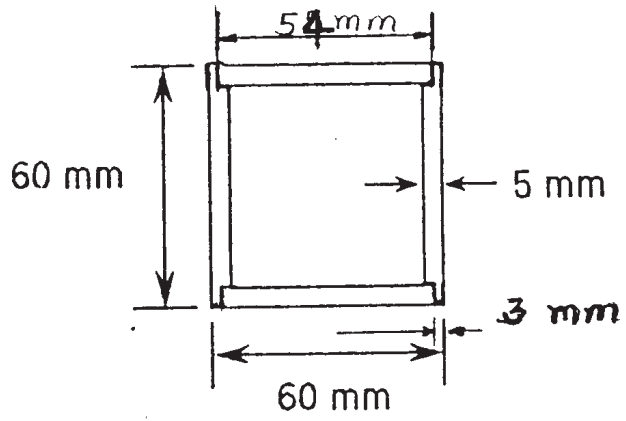

NOTES:

1. MATERIAL: FUSED SILICA

9/19/94

9/19/94

LONG BOLTS

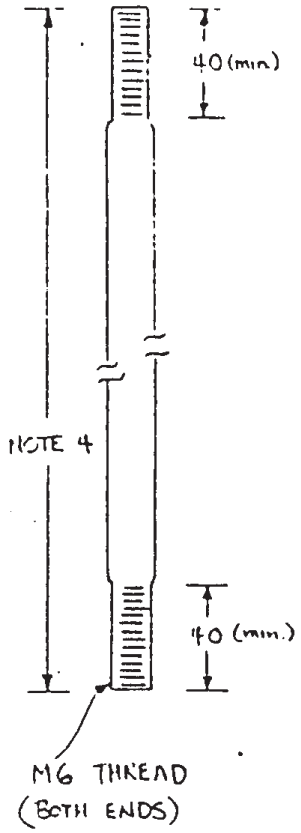

NOTES:

1) ALL UNITS IN MILLIMETER
2) DRAWING NOT TO SCALE
3) MATERIAL: STAINLESS STEEL - Φ6mm
4) LENGTH:

   350 - 4 PIECES

5) ALL TOLERANCE: ± 1mm

H4-2-1
John Chen
GR2

9/19/94

EXIT DIFFUSER (50 x 50 TUNNEL)

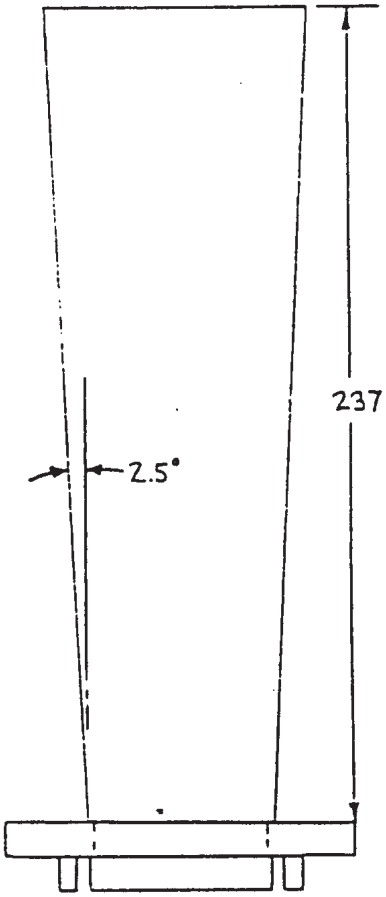

SECTION A-A

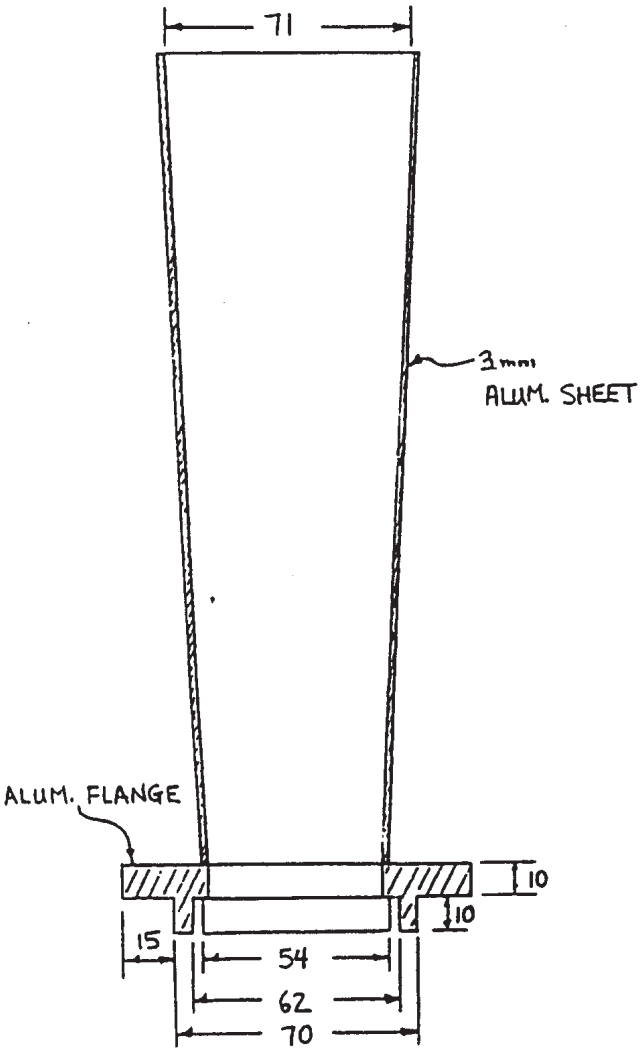

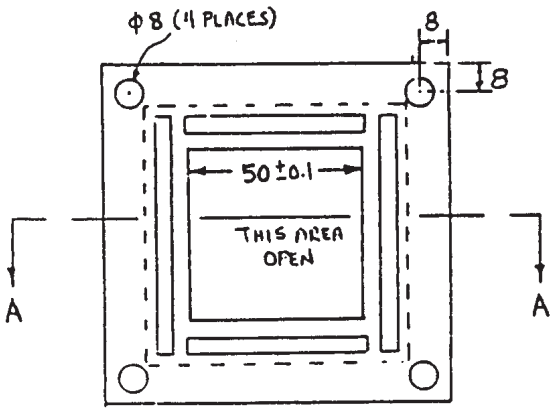

NOTES:

1) ALL UNITS IN MILLIMETER

2) EXTERNAL WELDS ONLY

3) ALL TOLERANCE : ± 0.25 mm, EXCEPT [illegible]

H4-2-1
John Chen
GRZ

B. Engineering drawings of wind tunnel

(NOTE: These drawings are available only in the hardcopy version of this report.)

C. Detailed experimental procedure

1. Place coal in oven and create vacuum pressure of approximately 29 in Hg and heat to 72^{o}C. Leave coal in oven for 24 hours.

Next Day:

1. Remove coal from oven. Turn the oven off.
2. Follow start-up procedure (on wall).
3. Turn on the air to the automatic feeder and gate.
4. Turn on the two pulse generators and the oscilloscope. Set laser control to program 2. Turn the bottom pulse generator to internal setting while simultaneously turning on the voltage supply.
5. Check to see if the lenses are aligned. Then check to see if the prisms are aligned correctly using the alignment rod. Make sure that the alignment rod is centered inside the quartz tunnel. If the prisms are not aligned adjust them till you can see that both of the beams are vertical to one another and intersect each other at the designated area of the alignment rod.
6. Turn on the gas flow of oxygen and nitrogen and set it to the selected flow rate and oxygen concentration.
7. Take coal out of oven and allow it to cool. Place the appropriate mesh size into the feeder and then pour the selected type coal on top of it.
8. Place and tighten the feeder inside the holder and line up the bottom of the holder to the blue line on the pole. Align feeder tube so that it is centered inside the quartz tunnel.

9. Place a light behind the outlet of the feeder tube and trigger the automatic feeder without firing the laser. Make sure that the back collar of the pneumatic trigger is what hits the feeder. This is done to create consistency in the experiment. Measure the time it takes the coal to exit the feeder and out of the feeder tube and reach the lasers height. View how far the coal particles drop before the gas flow pushes it back up. The coal should drop approximately 2 cm and take approximately 2.31 seconds.
10. Set the oscilloscope to record the ignition by pressing the run/stop button in the upper right hand corner. When the oscilloscope is ready the ready output should show a green light. To run experiment trigger the automatic feeder and gate by shifting the top pulse generator to external pulse and quickly shifting it back to single shot. Record whether there was an ignition or just a spark. Manually reset the feeder trigger.
11. Step 10 is repeated up to 19 times to complete a run.
12. After a run is completed clean the quarts tunnel. Tape a sheet of lens cleaning paper to the end of the cleaning tube and wet the sheet of paper with alcohol. Also blow the excess particles of coal out of the tunnel by turning of the oxygen and increasing the nitrogen flow rate.

After finishing experiment each day:

1. Cut off the power generator while simultaneously placing the bottom pulse generator on internal pulse.
2. Cut off both pulse generators and the oscilloscope.
3. Shut down procedure (on wall).
4. Cut off Nitrogen and Oxygen

5. Turn off the air to the automatic trigger and automatic gate.
6. Cover all optics and prisms with specified plastic bags.
7. Clean wind tunnel and then cover the wind tunnel opening with a plastic bag.
8. Cover the whole table with the large plastic covering.
9. Throw out used coal.

D. Ignition-frequency data in tabular format

Table D-1: Experiment Data for Pittsburgh #8 (DECS 23) Coal.

Size (μm)	63-75		106-125		150-180	
Oxygen Concentration (%)	E_{laser} (mJ)	Ignition Freq.	E_{laser} (mJ)	Ignition Freq.	E_{laser} (mJ)	Ignition Freq.
100	220 255 290 340	2/20 6/20 12/20 18/20	170 220 280 340	1/20 9/20 11/20 17/20	220 280 340 400	5/20 9/20 13/20 16/20
75	255 280 340 375	1/10 9/20 15/20 16/20	220 280 340 455 520	3/20 6/10 10/20 16/20 10/10	280 340 455 515	4/20 10/20 15/20 18/20
50	280 340 400 455	1/20 7/20 14/20 19/20	280 340 400 455 570	4/20 6/20 7/20 5/10 18/20	455 570 655 725	4/20 10/20 9/20 11/20

Table D-2: Experimental Data for Pittsburgh #8 DECS 23) Coal (second set).

Size (μm)	125-150					
Date:	7/30/97		8/7/97 & 8/13/97		9/3/97	
Oxygen Concentration (%)	E_{laser} (mJ)	Ignition Freq.	E_{laser} (mJ)	Ignition Freq.	E_{laser} (mJ)	Ignition Freq.
100	220 240 280 302.5 340	0/10 6/20 9/20 15/20 17/20	220 240 280 302.5 340	3/20 11/20 16/20 14/20 10/10	220 280 302.5 340	7/20 9/10 14/20 10/10
50	455 570 615 655 755	4/20 8/20 5/20 9/20 11/20	340 455 570	5/20 12/20 14/20	340 455 570	0/20 3/20 11/20

Table D-3: Experimental Data for Wyodak (DECS 26) Coal.

Size (μm)	63-75		106-125		150-180	
Oxygen Concentration (%)	E_{laser} (mJ)	Ignition Freq.	E_{laser} (mJ)	Ignition Freq.	E_{laser} (mJ)	Ignition Freq.
100	125	0/10	170	1/10	400	5/20
	170	3/20	220	7/20	455	9/20
	220	7/20	340	10/20	515	13/20
	280	8/20	455	9/10	570	17/20
	340	16/20	570	10/10		
50	340	3/20	460	0/20		
	455	5/20	655	3/20		
	570	8/20	725	4/20		
	655	12/20				
	725	16/20				
	742	16/20				

Table D-4: Experimental Data for Sewell (DECS 13) Coal.

Size (μm)	106 -125	
Oxygen Concentration (%)	E_{laser} (mJ)	Ignition Freq.
100	220	2/20
	255	8/20
	280	13/20
	340	16/20
75	220	2/20
	280	6/20
	340	9/20
	400	11/20
	455	16/20
50	455	4/20
	520	6/20
	620	6/20
	655	9/20
	700	10/20
	725	13/20

Table D-5: Experimental Data for Illinois #6 (DECS 24) Coal.

Size (μm)	106-125	
Oxygen Concentration (%)	E_{laser} (mJ)	Ignition Freq.
100	220	3/20
	340	8/20
	460	14/20
	520	15/20
	570	10/10
50	655	0/20
	725	3/20
	755	6/20